NASA TECHNICAL NOTE

NASA TN D-2388

NASA TN D-2388

VECTORIAL REFLECTANCE OF THE EXPLORER IX SATELLITE MATERIAL

by Gerald M. Keating and James A. Mullins

Langley Research Center
Langley Station, Hampton, Va.

NATIONAL AERONAUTICS AND SPACE ADMINISTRATION • WASHINGTON, D. C. • AUGUST 1964

32

VECTORIAL REFLECTANCE OF THE EXPLORER IX SATELLITE MATERIAL

By Gerald M. Keating and James A. Mullins

Langley Research Center
Langley Station, Hampton, Va.

NATIONAL AERONAUTICS AND SPACE ADMINISTRATION

For sale by the Office of Technical Services, Department of Commerce,
Washington, D.C. 20230 -- Price $1.25

VECTORIAL REFLECTANCE OF THE EXPLORER IX SATELLITE MATERIAL

By Gerald M. Keating and James A. Mullins
Langley Research Center

SUMMARY

Reflectance measurements were made at different azimuth and colatitude angles relative to flat samples of the aluminum and white epoxy paint surfaces used on the Explorer IX satellite by means of an adapted monoplanar goniophotometer. Contour charts of the reflectance from these samples were obtained from the results of these measurements. Reflectance relative to mutually perpendicular axes was obtained by graphical integration of the contour charts. The vectorial summation of the reflectance was thus obtained. The aluminum sample was found to be essentially a specular reflector and the white epoxy paint sample was found to be essentially a diffuse reflector.

INTRODUCTION

The Explorer IX satellite (refs. 1 and 2) is used to infer atmospheric density at perigee altitudes from the energy decay of the satellite. Since the energy changes of the satellite due to solar radiation forces through most of its lifetime have been of the same order of magnitude as the energy decay due to aerodynamic drag, it is essential for accurate determination of density that the solar radiation force upon the satellite be known.

The radiation force upon the satellite could have been determined by measuring the forces on irradiated satellite material by means of a torsion balance. Unfortunately, no instrument of sufficient precision was available; thus, a study of the reflective characteristics of the material, from which the radiation force may be easily deduced was required.

The determination of the rate of momentum transfer or force due to incidence of parallel photons is quite straightforward. (See ref. 3.) The reaction force produced by the reflection of photons is not solely dependent on the fraction of photons reflected or hemispherical reflectance, but in addition, on the directions at which photons are reflected. Therefore, the force due to reflection of light is dependent on the vectorial summation of the reflected light or vectorial reflectance.

The results of a literature survey did not yield a previous determination of reflectance as a function of azimuth and colatitude for Explorer IX material nor were equations available which accurately predict the amount of light reflected in each direction. It was, therefore, considered necessary to obtain →

measurements of the spatial distribution of reflected light from samples of the Explorer IX material at different angles of incidence so that momentum exchange due to reflection could be more accurately evaluated. These measurements were made under contract to the National Aeronautics and Space Administration by the National Bureau of Standards (NBS). This report describes the measurements that NBS was requested to make and presents the analysis made at the NASA Langley Research Center.

SYMBOLS

A	area, cm^2
c	speed of light in vacuum, cm $(sec)^{-1}$
f	focal length, cm
$\vec{F}$	force, dynes
H	incident power per unit area normal to direction of propagation, erg $(cm)^{-2}(sec)^{-1}$
$h\nu$	energy of a photon (Planck's constant times the frequency of the photon), ergs
i	angle of incidence, deg
$\vec{i}$	unit vector along positive X-axis of figure 1
$\vec{j}$	unit vector along positive Y-axis of figure 1
$\vec{J}(\phi,\psi)$	radiant intensity of reflected light in direction ϕ,ψ (eq. (8)), ergs $(steradian)^{-1}(sec)^{-1}$
J	radiant intensity of reflected light, ergs $(steradian)^{-1}(sec)^{-1}$
$\vec{k}$	unit vector along positive Z-axis of figure 1
$\vec{L}$	unit vector denoting direction of photon
m,n	integers
$\vec{P}$	vectorial summation of radiant power, ergs $(sec)^{-1}$
P_I	magnitude of parallel incident power, ergs $(sec)^{-1}$
$P_{S,2.5}$	radiant power reflected within 2.5° of angle of specular reflection, ergs $(sec)^{-1}$

$\vec{r}$ vectorial reflectance (eq. (5))

R_n reflectance per unit solid angle normal to sample, $(\text{steradian})^{-1}$

$\vec{R}(\phi,\psi)$ reflectance per unit solid angle in direction ϕ,ψ (eq. (12)), $(\text{steradian})^{-1}$

$\vec{S}$ unit vector in direction of specular reflection, unitless

X,Y,Z coordinate axes

α angle measured clockwise in plane of measurement (that plane defined by optical axes of light source and photometer) from light source to photometer (fig. 5), deg

α_n angle measured clockwise in plane of measurement (that plane defined by optical axes of light source and photometer) from light source to projection of normal to sample (fig. 6), deg

α' angle measured clockwise in plane of measurement (that plane defined by optical axes of light source and photometer) from projection of normal to sample to photometer (arc MP of fig. 6), deg

β angle measured clockwise in plane of measurement (that plane defined by optical axes of light source and photometer) from light source to right horizontal axis of rotation of sample (fig. 5), deg

γ tilt angle of sample plane (fig. 5), deg

η angle between plane of measurement (that plane defined by optical axes of light source and photometer) and X,Z plane of figure 1 (fig. 6), deg

θ angle of vectorial reflection, measured in X,Z plane of figure 1 from -Z toward -X, deg

ϕ colatitude angle measured from normal to sample (fig. 1), deg

ψ azimuth angle measured as shown in figure 1, deg

Ω solid angle, steradian

Subscripts:

D diffused component of light

i summation index

I incident light

R reflected light

S specular component of light

ϕ at angle ϕ

n normal to sample

THEORY OF RADIATION FORCE

The coordinate system used in this discussion is illustrated in figure 1. The X,Y plane is in the plane of the sample, with the X-axis along the projection of the incident ray on the sample plane. The sample is placed on an opaque sample holder, which permits illumination of only one side of the sample. The -Z-axis is normal to the illuminated side of the sample. The X,Z plane contains the incident ray and is called the incident plane.

Some angles pertinent to the discussion are shown in figure 1. The angle of incidence is defined as the angle between the normal to the material and the incident ray. Positions at which measurements are made are expressed in terms of the colatitude angle ϕ measured from the -Z axis, and the azimuth angle ψ, measured from the plane of incidence in a clockwise sense about the -Z axis to the plane containing ϕ.

If $h\nu_i/c$ is the magnitude of momentum of the ith photon and $\vec{L}_i$ is a unit vector in the direction of propagation of the ith photon, the summation of momenta of n photons may be expressed as

$$\sum_{i=1}^{n} \frac{h\nu_i}{c} \vec{L}_i \tag{1}$$

Consider a flux of n photons per unit time incident upon flat surface A. Then the momentum flux or force $\vec{F}_I$ upon surface A due to incidence of photons, excluding the additional momentum transfer due to reflection, is

$$\vec{F}_I = \frac{1}{c} \sum_{i=1}^{n} h\nu_i \vec{L}_i = \frac{1}{c} \vec{P}_I \tag{2}$$

where $\vec{P}_I$ is the vectorial summation of incident radiant power.

Similarly, if m photons per unit time are reflected from surface A, the reaction force $\vec{F}_R$ upon the surface due only to the reflection of photons is

$$\vec{F}_R = -\frac{1}{c}\sum_{i=1}^{m} h\nu_i \vec{L}_i = -\frac{1}{c}\vec{P}_R \tag{3}$$

where $\vec{P}_R$ is the vectorial summation of reflected radiant power.

The total radiation force $\vec{F}$ acting on surface A, thermal emission being neglected, is given by the vectorial summation of forces due to incidence and reflection.

$$\vec{F} = \vec{F}_I + \vec{F}_R = \frac{1}{c}\left(\vec{P}_I - \vec{P}_R\right) \tag{4}$$

It is convenient to determine radiation force in terms of the vectorial reflectance of a material $\vec{r}$ which is assumed to be dependent on the direction but not on the magnitude of the incident radiant power. Vectorial reflectance is defined for parallel incident light and is the vectorial summation of reflected radiant power divided by the magnitude of the incident radiant power.

$$\vec{r} \equiv \frac{\vec{P}_R}{P_I} \tag{5}$$

where P_I is the magnitude of parallel incident radiant power. In the case under consideration where all incident power is parallel, the radiation force on area A is

$$\vec{F} = \frac{P_I}{c}\left(\vec{L}_I - \vec{r}\right) \tag{6}$$

where $\vec{L}_I$ is a unit vector in the direction of the incident light. P_I may be measured in terms of the incident power per unit area H and $\vec{r}$ may be measured in terms of the radiant intensity of reflected light in each direction $\vec{J}(\phi,\psi)$. If parallel light of measured power per unit area H is incident at angle of incidence i on area A, then

$$P_I = H(\cos i)A \tag{7}$$

Let $\vec{J}(\phi,\psi)$ represent the measured reflected power per unit solid angle reflected in direction ϕ,ψ.

$$\vec{J}(\phi,\psi) \equiv \frac{d\vec{P}_R}{d\Omega} \tag{8}$$

where $d\Omega$ is a differential solid angle.

It is convenient to determine $\vec{r}$ in terms of $\vec{R}(\phi,\psi)$, where

$$\vec{R}(\phi,\psi) = \frac{d\vec{r}}{d\Omega} = \frac{\vec{J}(\phi,\psi)}{P_I} \tag{9}$$

in light of this definition,

$$\vec{r} = \int_{\phi=0}^{\phi=\frac{\pi}{2}} \int_{\psi=0}^{\psi=2\pi} \vec{R}(\phi,\psi) \sin\phi \, d\phi \, d\psi \tag{10}$$

Define mutually perpendicular unit vectors $\vec{i}$, $\vec{j}$, and $\vec{k}$ along the positive X, Y, and Z axes, respectively, shown in figure 1. Then

$$\vec{R}(\phi,\psi) = \left|\vec{R}(\phi,\psi)\right|\left[\sin\phi \, (\cos\psi) \, \vec{i} + \sin\phi \, (\sin\psi) \, \vec{j} - (\cos\phi) \, \vec{k}\right] \tag{11}$$

Substituting equation (11) into equation (10) yields

$$\vec{r} = \vec{i} \int_{\phi=0}^{\phi=\frac{\pi}{2}} \int_{\psi=0}^{\psi=2\pi} \left|\vec{R}(\phi,\psi)\right| \sin^2\phi \cos\psi \, d\phi \, d\psi$$

$$+ \vec{j} \int_{\phi=0}^{\phi=\frac{\pi}{2}} \int_{\psi=0}^{\psi=2\pi} \left|\vec{R}(\phi,\psi)\right| \sin^2\phi \sin\psi \, d\phi \, d\psi$$

$$- \vec{k} \int_{\phi=0}^{\phi=\frac{\pi}{2}} \int_{\psi=0}^{\psi=2\pi} \left|\vec{R}(\phi,\psi)\right| \sin\phi \cos\phi \, d\phi \, d\psi \tag{12}$$

If symmetry with respect to the $\vec{i},\vec{k}$ plane is assumed,

$$\vec{j} \int_{\phi=0}^{\phi=\frac{\pi}{2}} \int_{\psi=0}^{\psi=2\pi} \left|\vec{R}(\phi,\psi)\right| \sin^2\phi \sin\psi \, d\phi \, d\psi = 0 \tag{13}$$

Finally,

$$\vec{L_I} = -(\sin i)\vec{i} + (\cos i)\vec{k} \tag{14}$$

APPARATUS

Test Samples

The Explorer IX satellite (fig. 2) is essentially a spherical balloon made of a four-ply laminate of alternate layers of 0.5-mil (0.00127 cm) 1145 aluminum and plastic film with the aluminum surface on the outside of the balloon. Two-inch-diameter (5.08 cm) dots of white epoxy paint uniformly cover 18 percent of the 12-foot-diameter (365.76 cm) aluminum surface. Therefore, samples of the four-ply laminate and of the four-ply laminate coated with white epoxy paint were prepared. The paint, a white epoxy enamel, was sprayed onto the aluminum samples to the consistency used on Explorer IX and then cured by baking for 1 hour at 300° F (422° K).

The aluminum and white paint samples were glued to flat aluminum-alloy plates 5 inches × 5 inches × 1/4 inch (12.70 cm × 12.70 cm × 0.635 cm) in vacuo to minimize the number of dust particles being trapped beneath the samples.

Goniophotometer

The apparatus used to measure the distribution of reflected light was the NBS manual monoplane goniophotometer. (See ref. 4.) The instrument is composed of three parts: the source unit, the sample housing, and the collector unit. It may be seen in figure 3 that light passes from a 2,854° K tungsten source through a focusing lens whose focal point is at a variable source aperture (2.5 mm in diameter) which is also at the focal point of the collimating lens (f = 114 mm). The light passes through the collimating lens and the resultant beam of parallel light, limited by a circular aperture diaphragm to 3 centimeters in diameter, is reflected from the sample. In order to measure the intensity of light at a given angle of reflection, a collector lens (f = 536 mm) which sees the entire illuminated portion of the sample focuses all light reflected at a given angle upon a receiver aperture. The reflected light passing through the receiver aperture is then measured by means of a photometer unit. The small solid angle subtended by the receiver aperture is the receiver aperture area divided by the square of the focal length of the collector lens.

The photometer unit used throughout the measurements employed an a-c modulated blue sensitive S-4 phototube and an a-c amplifier. The photometer was found to have a linear response over the range of values measured.

A photograph of the apparatus is shown in figure 4. The collector unit and specimen holder are free to rotate about a vertical axis passing through the center of the sample. The collector unit is limited to 330° rotation and the specimen holder may rotate 360°. Normally, a monoplanar goniophotometer can measure reflectance only in the plane defined by the optical axis of the source unit and a normal passing through the center of the sample. In order that reflectances could be measured in any plane, the sample housing was modified so that the specimen holder could rotate 360° about a horizontal axis in the plane of the sample passing through its center.

For the diffusely reflected light, the intensity was low enough to allow the phototube to be placed directly behind an 8-millimeter-diameter receiver aperture. It was assumed for the measurements made that the reflectance per unit solid angle measured was the reflectance per unit solid angle at the center of the solid angle subtended.

In order to measure the intensity of light in the vicinity of specular reflection, the phototube could no longer be placed directly behind the receiver aperture and was, therefore, placed on the side of an 8-inch-diameter (20.32 cm) $BaSO_4$ coated diffusing sphere shown in figure 4.

The light in the vicinity of specular reflection was measured by centering the receiver aperture on the specular peak. Six circular apertures subtending half-angles of 0.5°, 0.75°, 1°, 1.5°, 2°, and 2.5° were used. By making such measurements with circular receiver apertures of different diameters, the differences in the power received could be used to determine the variation of radiant intensity in the immediate region of specular reflection.

The photometer was calibrated for diffuse reflectance measurements by measuring light reflected normally from a magnesium oxide plaque illuminated with light incident at 45°. At this particular angle of reflection, the same amount of light is reflected as from a perfectly reflecting, perfectly diffusing reflector. Therefore, the theoretical reading for the incident beam could be deduced. The photometer was calibrated for specular reflectance measurements by taking a direct reading of the incident beam.

MEASUREMENTS

Determination of Representative Angles of Incidence and Reflection

In order to minimize the number of measurements necessary to determine the reflective properties of the Explorer IX material, representative angles of incidence and reflection were chosen.

The projected area of the spherical satellite was divided into five equal concentric areas about the satellite-sun line upon each of which an equal amount of solar energy is incident. A circle was chosen for each projected annular area such that half of the area and thus one-half the solar energy fell on each side of the circle. The angles of incidence corresponding to the radii of these circles were chosen as those to be investigated. It follows that the angles of incidence i are given by the equation

$$i = \arcsin\left(\frac{2n - 1}{10}\right)^{1/2} \qquad (n = 1,2,3,4,5) \qquad (15)$$

It was assumed that the diffuse reflection pattern follows the Lambert cosine law

$$J_{\phi} = J_n \cos \phi \tag{16}$$

where J_n and J_{ϕ} are reflected intensities normal to the sample and at angle ϕ, respectively.

An imaginary hemisphere was constructed about an illuminated elemental area. Four concentric zones were constructed on the hemisphere such that each zone contained one-quarter of the diffusely reflected light if a Lambertian distribution is assumed. A colatitude angle was chosen for each zone such that half the light reflected through each zone was above and half below the colatitude angle. The colatitude angles ϕ may be written as

$$\phi = \text{arc sin}\left(\frac{2n - 1}{8}\right)^{1/2} \qquad (n = 1,2,3,4) \tag{17}$$

To minimize the number of measurements, it was assumed that the reflection of light was symmetrical about the plane defined by the incident ray and the normal to the material. Therefore, azimuth angles ψ were selected only between 0° to 180°. In accordance with the Lambert cosine law, the diffuse reflectance was assumed to be independent of azimuth angle. Therefore, each concentric area was divided into four segments between $\psi = 0^{\circ}$ and 180°, and each segment was of the same angular extent in azimuth. An average azimuth angle was chosen midway between the extremities of each segment. Therefore, azimuth angles were chosen as follows:

$$\psi = \left(\frac{2n - 1}{8}\right)180^{\circ} \qquad (n = 1,2,3,4) \tag{18}$$

All combinations of inclination, azimuth angle, and colatitude angle discussed were investigated to determine the diffuse reflection properties of the aluminum and white epoxy paint and for each material constituted 80 measurements.

In order to investigate the specular reflection from each sample, the area in the immediate vicinity of the angle of specular reflection was investigated. The angle of specular reflection is at a colatitude angle equivalent to the angle of incidence and at an azimuth angle of 180°.

In order to investigate the transition region between specular and diffuse reflection, measurements were made in the near vicinity of specular reflection along the plane defined by the incident ray and the normal to the material, and including the specularly reflected ray.

Apparatus Settings

Apparatus settings of the angles α, β, and γ may be calculated so that the sample is properly oriented relative to the light source and photometer for the required angles of i, ϕ, and ψ.

Shown in figure 5 is a schematic diagram of the apparatus settings of the goniophotometer. The optical axes of the light source and photometer define the plane of measurement. The angle α is measured clockwise from the optical axis of the light source to the optical axis of the photometer. The angle β is measured clockwise in the plane of measurement from the optical axis of the light source to the right horizontal axis of rotation of the sample holder. In order that reflectances may be measured outside of the plane defined by the optical axis of the light source and the normal to the material, an adaption was made to the instrument such that the sample could be tilted relative to the vertical axis of rotation. The tilt angle γ is measured from the vertical axis of rotation to the axis in the plane of the sample which is normal to the horizontal axis of rotation. In order that the sample side of the specimen plane may be seen simultaneously by the light source and photometer, and since $0 \leqq \psi \leqq 180^\circ$,

$$180^\circ \leqq \beta \leqq 360^\circ \tag{19}$$

$$0 \leqq \alpha \leqq 180^\circ \tag{20}$$

$$0 \leqq \gamma \leqq 90^\circ \tag{21}$$

Figure 6 is a schematic diagram of the light source L and photometer P relative to the sample plane X,Y. Angles α, α_n, and γ correspond, respectively, to arcs LP, LM, and NM, which are all portions of great circles on a hemisphere constructed about the center of the sample, denoted by point O. Angles α and γ have been previously described in figure 5. The angle α_n is measured clockwise relative to -Z, the normal to the material, from the optical axis of the light source OL to OM, the projection of the normal to the material on the plane of measurement. It may be seen in figure 6 that

$$\beta = \alpha_n - 90^\circ \tag{22}$$

The angle α is determined from the oblique spherical triangle LPN. By the law of cosines,

$$\cos \alpha = \cos i \cos \phi + \sin i \sin \phi \cos \psi \tag{23}$$

Therefore,

$$\alpha = \arccos(\cos i \cos \phi + \sin i \sin \phi \cos \psi) \tag{24}$$

where from equation (20)

$$0 \leqq \alpha \leqq 180^\circ$$

The angle γ may be determined from the right spherical triangle LMN as follows:

$$\sin \gamma = \sin \eta \sin i \tag{25}$$

The angle η may be determined from the oblique spherical triangle LPN. By the law of sines,

$$\frac{\sin \eta}{\sin \phi} = \frac{\sin \psi}{\sin \alpha} \tag{26}$$

Substituting equation (26) into equation (25) and solving for γ,

$$\gamma = \arcsin\left(\frac{\sin \psi \sin \phi \sin i}{\sin \alpha}\right) \tag{27}$$

where from equation (21)

$$0 \leqq \gamma \leqq 90^\circ$$

The angle α_n may be determined from the right spherical triangle LMN as follows:

$$\cos i = \cos \alpha_n \cos \gamma \tag{28}$$

and

$$\cos \alpha_n = \frac{\cos i}{\cos \gamma} \tag{29}$$

Since equation (29) yields two values of α_n between $-\pi/2$ and $\pi/2$, further calculations must be made in order to determine α_n uniquely.

Let

$$\alpha = \alpha_n + \alpha' \tag{30}$$

where α' is defined to be the arc MP. From the right spherical triangle MPN,

$$\cos \phi = \cos \alpha' \cos \gamma \tag{31}$$

and

$$\alpha' = \text{arc cos} \frac{\cos \phi}{\cos \gamma} \tag{32}$$

Equation (32) yields two values of α' between $-\pi/2$ and $\pi/2$.

Although α_n and α' given by equations (29) and (32) are double-valued, only one combination of values will satisfy equation (30) and β can then be determined from equation (22).

ANALYSIS

The measured values of reflectance in the plane of incidence and in planes perpendicular to the sample displaced by 22.5° and 67.5° from the plane of incidence for both the white paint and aluminum samples along with contour plots obtained by crossplotting and fairing between the measured values are presented in figures 7 to 26 for angles of incidence of 18.4°, 33.2°, 45.0°, 56.8°, and 71.6°. The planar reflectance data are presented as a ratio of $\frac{\vec{R}(\phi,\psi)}{R_n}$ (designated $\frac{R}{R_n}$ on figs.) and the contour plots are presented in terms of $\vec{R}(\phi,\psi)$ (designated R). The measured values of R_n plotted against angle of incidence are presented in figure 27. The data were then evaluated for $\vec{r}$ by letting $\vec{r}_S$ be the vectorial reflectance within a cone of 2.5° of the angle of specular reflection and $\vec{r}_D$ be the vectorial reflectance of the remaining light. Then

$$\vec{r} = \vec{r}_S + \vec{r}_D \tag{33}$$

where

$$\vec{r}_S = \frac{P_{S,2.5}\vec{S}}{P_I} \tag{34}$$

It was assumed that the light in the 2.5° half-angle cones is essentially parallel. The term $\vec{r}_D$ is evaluated by graphically integrating equation (12), $R(\phi,\psi)$ dropping to zero at an angle of 2.5° from $\vec{S}$, and the integration for $\vec{r}_D$ being carried out in two steps. First, $\vec{R}(\phi,\psi)\sin^2\phi$ and $\vec{R}(\phi,\psi)\sin\phi\cos\phi$ were graphically integrated with respect to ϕ for constant values of ψ. Integrals could be immediately obtained from the measured values for ψ = 0°, 22.5°, 67.5°, 112.5°, 157.5°, and 180° and additional integrals were determined from the contour plots. The integrals of ϕ, multiplied by $\cos\psi$ for the $\vec{i}$ component, were plotted against ψ and graphically integrated a second time, to obtain the components of $\vec{r}_D$ along the X- and Z-axes. By summing the components of $\vec{r}_D$ and $\vec{r}_S$ along the X- and Z-axes, the direction θ and the magnitude $|\vec{r}|$ of $\vec{r}$ were obtained.

RESULTS AND DISCUSSION

Shown in figure 27 is the magnitude of reflectance per unit solid angle normal to the surface R_n as a function of angle of incidence i for the aluminum and white paint samples. As may be seen, R_n decreases more rapidly at low angles of incidence for aluminum but decreases more rapidly at high angles of incidence for white epoxy paint. For both aluminum and white paint, the total diffuse reflection decreased with angle of incidence.

Shown in figure 7 are values of $\vec{R}(\phi,\psi)/R_n$ as a function of ϕ for planes perpendicular to the white epoxy paint sample for an angle of incidence of 18.4°. The dotted lines show the reflection pattern of a diffuse reflector following the Lambert cosine law (eq. (16)). Figure 7(a) shows values of $\vec{R}(\phi,\psi)/R_n$ in the incident plane which passes through ψ = 0° and ψ = 180°, which by definition is the plane containing the incident ray and a normal to the sample. The polar-log plot shows data points obtained from both specular and diffuse measurements. Specular measurements are those in which the $BaSO_4$ coated diffusing sphere was used. Diffuse measurements are those in which the phototube was mounted directly behind the receiver aperture. As may be seen, the value obtained at the angle of specular reflection (ϕ = 18.4°) is orders of magnitude greater than the value at the normal which is defined as 1.

In figure 7(b), $\vec{R}(\phi,\psi)/R_n$ is shown as a function of ϕ for a plane perpendicular to the sample but 22.5° away from the plane of incidence. Because of symmetry with respect to the incident plane, measurements at azimuth ψ are

equal to measurements at azimuth $-\psi$. The polar plot shows only points obtained from diffuse reflectance measurements. Note the high value of $\vec{R}(\phi,\psi)/R_n$ at $\phi = 21.7^\circ$ which is in the near vicinity of the specular peak.

The measurement plane (fig. 7(c)) is 67.5° from the plane of incidence. Here, the data points more closely follow the Lambert cosine law.

In figure 8 are shown contours of $\vec{R}(\phi,\psi)$ plotted as a function of ϕ and ψ. This plot was obtained by cross plotting the curves of figure 7. The general reflection pattern may be seen at once. The circular contours show reflectance essentially independent of azimuth angle ψ, except in the region of specular reflection where a peak occurs. Although the peak is very high, it occurs over a small solid angle.

Figures 9 and 10 are similar to figures 7 and 8 except that they are obtained for an angle of incidence of 33.2°. By comparing figures 8, 10, 12, 14, and 16, it is seen that the specular peak has increased in angular extent and magnitude with an increase in the angle of incidence.

As in the contours for white paint, the aluminum contours (figs. 18, 20, 22, 24, and 26) show regions of intense reflected light occurring about the angle of specular reflection. However, although there is diffusely reflected light, there is no discernible Lambertian pattern for aluminum. There appear two ridges of intensity in each aluminum contour: one along the plane of incidence, and a circular ridge occurring at $\phi = i$. Furthermore, it was noticed that a visible cross pattern occurred when light reflected from the sample was projected on a screen. It was suggested by the National Bureau of Standards that this effect was probably due to the cross grain of the material.

Values of $\vec{R}(\phi,\psi)/R_n$ are given as a function of ϕ for the aluminum sample for an angle of 18.4° in figure 17(a). The circular reflection pattern of the diffuse reflector is no longer noticeable. Scanning all the data of $\vec{R}(\phi,\psi)/R_n$ in the (b) and (c) parts of figures 17, 19, 21, 23, and 25 indicates that a maximum measured value occurs in each plane at the point closest to $\phi = i$. As a result, the curves were drawn with peaks at $\phi = i$. Other peaks occur in the vicinity of the normal to the sample where peaks occur for Lambertian diffuse reflection.

In figure 28 is shown a plot of the total reflectance within 2.5° of the angle of specular reflection for aluminum and white epoxy paint. As may be seen, specular reflection for both aluminum and white epoxy paint increases with angle of incidence. The curve for white paint increases slope more rapidly as grazing incidence is approached.

In figure 29 is shown a plot of reflectance per unit solid angle at the infinitesimal solid angle subtended at the specular peak. These extrapolated values were obtained by plotting reflectance per unit solid angle as a function of aperture angle subtended for five concentric apertures about the specular peak. The reflectance per unit solid angle at the specular peak increases more rapidly with angle of incidence than does $\vec{r}_s$ of the previous figure.

In figure 30 is plotted $\vec{r}$, total vectorial reflectance, in terms of the magnitude and direction as a function of the angle of incidence for aluminum and white epoxy paint. The magnitude of vectorial reflectance increases with angle of incidence after 33.2° for aluminum, but remains essentially constant for white paint. The direction of vectorial reflectance for the aluminum sample is never greater than 1° from the direction of specular reflection. For low angles of incidence, the vectorial reflectance of white epoxy paint is practically normal to the surface.

The errors due to measurement of $|\vec{r}_S|$ are estimated to be less than 5 percent. The errors in $|\vec{r}_D|$ due to measurement and integration are estimated to be less than 1 percent because of the cancellation of random measurement errors. The directions of $\vec{r}_S$ and $\vec{r}_D$ are accurate to within 10 minutes of arc and therefore the inaccuracy in the direction of $\vec{r}$ is primarily due to the inaccuracy in $|\vec{r}_S|$. Adding $\vec{r}_S$ and $\vec{r}_D$ to obtain $\vec{r}$ yields errors of less than 5 percent for $|\vec{r}|$.

CONCLUSIONS

Based on the data obtained with the Explorer IX satellite material, the following conclusions can be drawn:

1. For both the aluminum and the white epoxy paint samples, diffuse reflection decreases with angle of incidence and specular reflection increases with angle of incidence.

2. The white epoxy paint sample is essentially a diffuse reflector with a superimposed specular peak.

3. The aluminum sample is essentially a specular reflector with a small diffuse component.

4. Vectorial reflectance of the aluminum sample increases with angle of incidence and is within 1° of the direction of specular reflection.

5. Vectorial reflectance of white paint varies slowly with angle of incidence over the range measured. At low angles of incidence, the direction of vectorial reflectance is nearly normal to the surface. End

Langley Research Center,
National Aeronautics and Space Administration,
Langley Station, Hampton, Va., April 20, 1964.

REFERENCES

1. Coffee, Claude W., Jr., Bressette, Walter E., and Keating, Gerald M.: Design of the NASA Lightweight Inflatable Satellites for the Determination of Atmospheric Density at Extreme Altitudes. NASA TN D-1243, 1962.

2. Woerner, Charles V., and Keating, Gerald M.: Temperature Control of the Explorer IX Satellite. NASA TN D-1369, 1962.

3. O'Sullivan, William J., Jr., Coffee, Claude W., Jr., and Keating, Gerald M.: Air-Density Measurements From the Explorer IX Satellite. Space Research III, Wolfgang Priester, ed., North-Holland Publ. Co. (Amsterdam), 1963, pp. 89-95.

4. Hammond, Harry K., III, and Nimeroff, Isadore: Measurement of Sixty-Degree Specular Gloss. NBS Research Paper RP2105, U.S. Dept. Commerce Jour. Research of National Bur. Standards, vol. 44, June 1950, pp. 585-598.

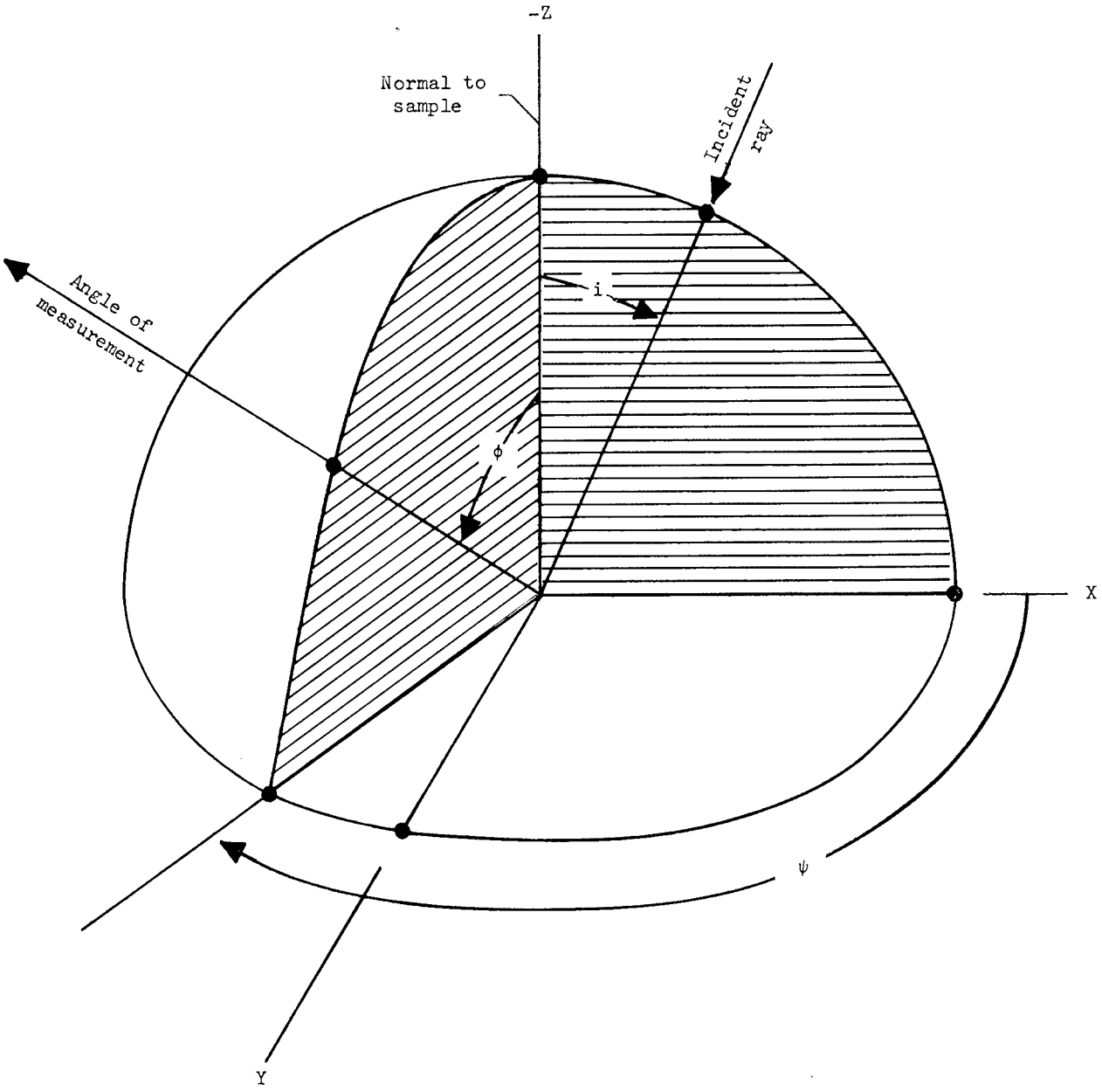

Figure 1.- Figure illustrating coordinate system.

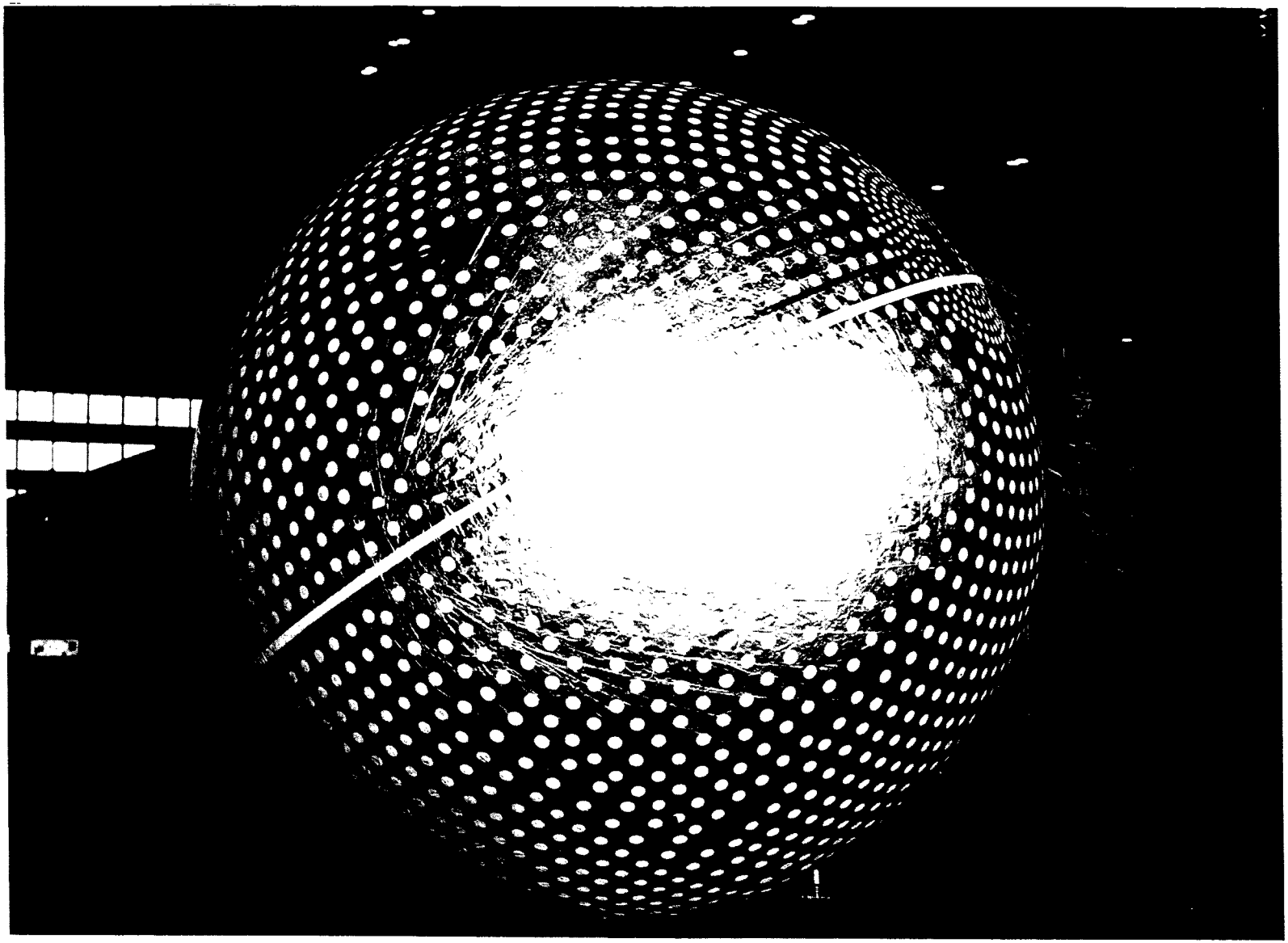

Figure 2.- Explorer IX satellite. L-61-3762

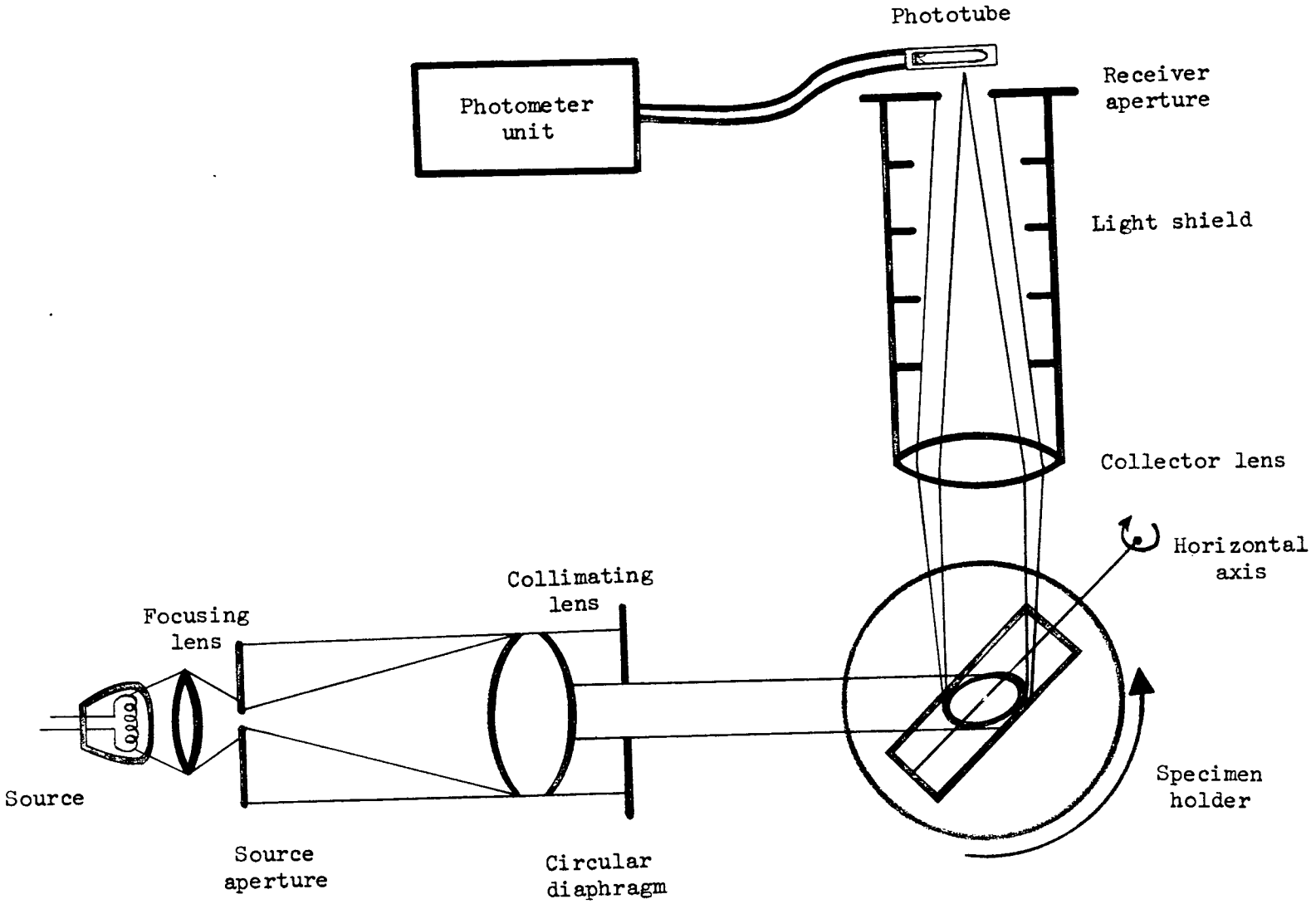

Figure 3.- Schematic diagram of goniophotometer.

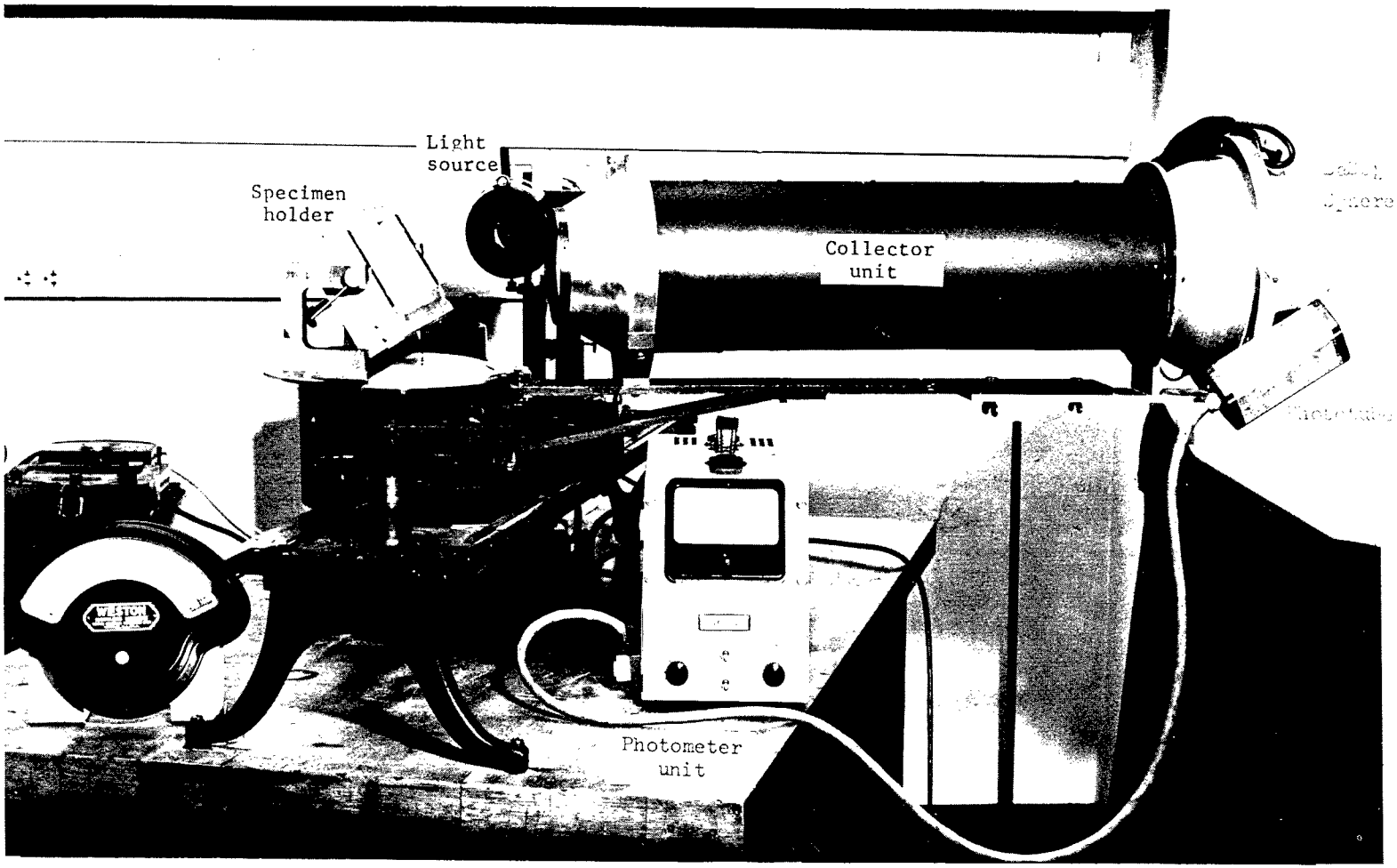

Figure 4.- Photograph of goniophotometer. L-64-3058

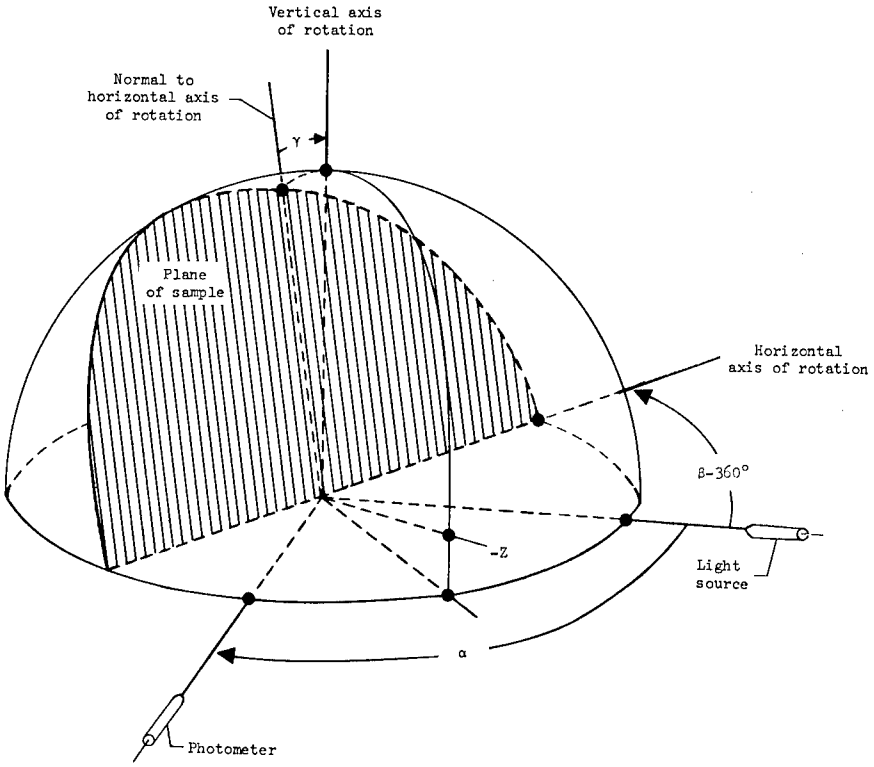

Figure 5.- Schematic diagram of apparatus settings of the goniophotometer

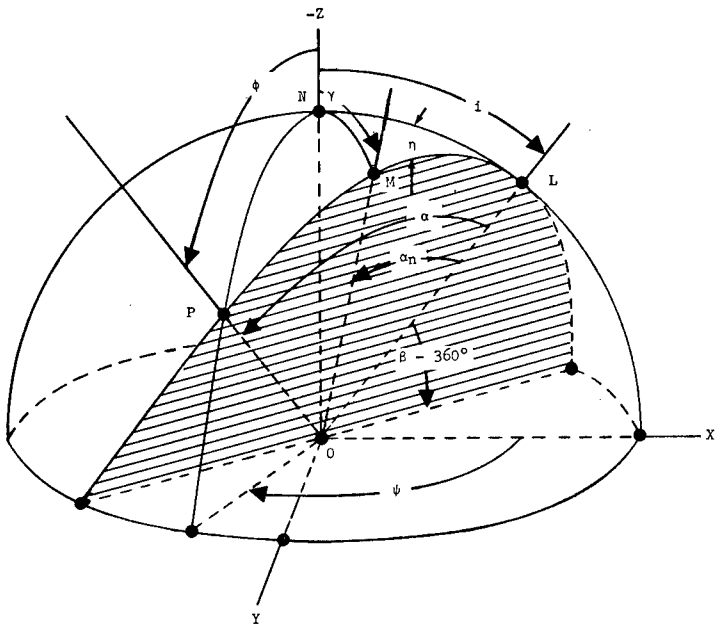

Figure 6.- Schematic diagram of light source and photometer relative to the sample plane.

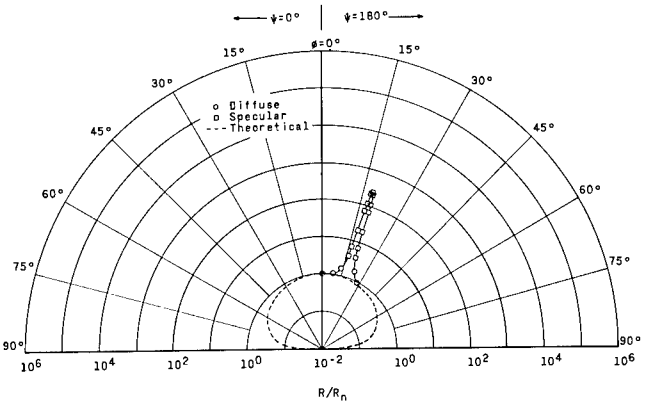

(a) Reflectance in plane of incidence.

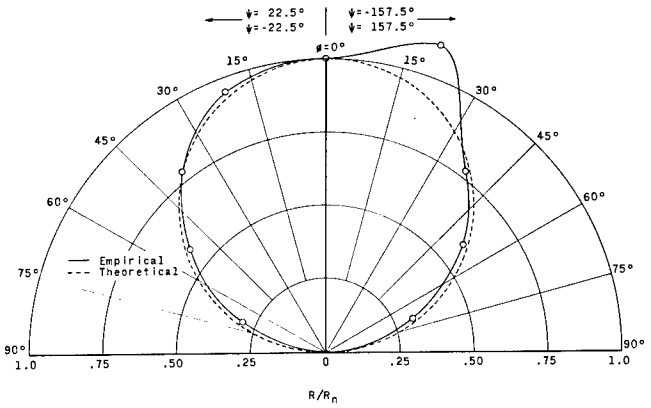

(b) Reflectance in plane displaced 22.5° from plane of incidence.

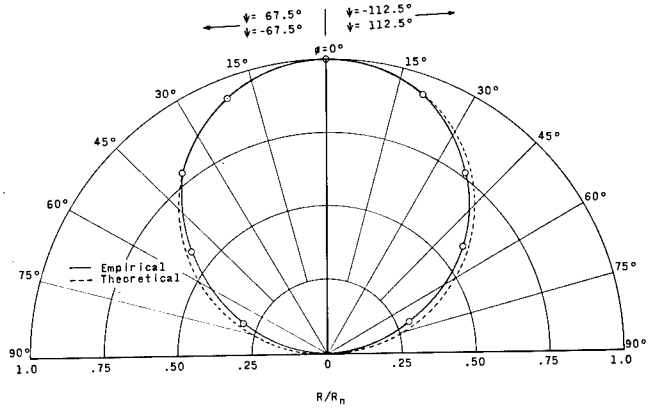

(c) Reflectance in plane displaced 67.5° from plane of incidence.

Figure 7.- Planar reflectance of white paint as a function of ϕ for $i = 18.4^{\circ}$.

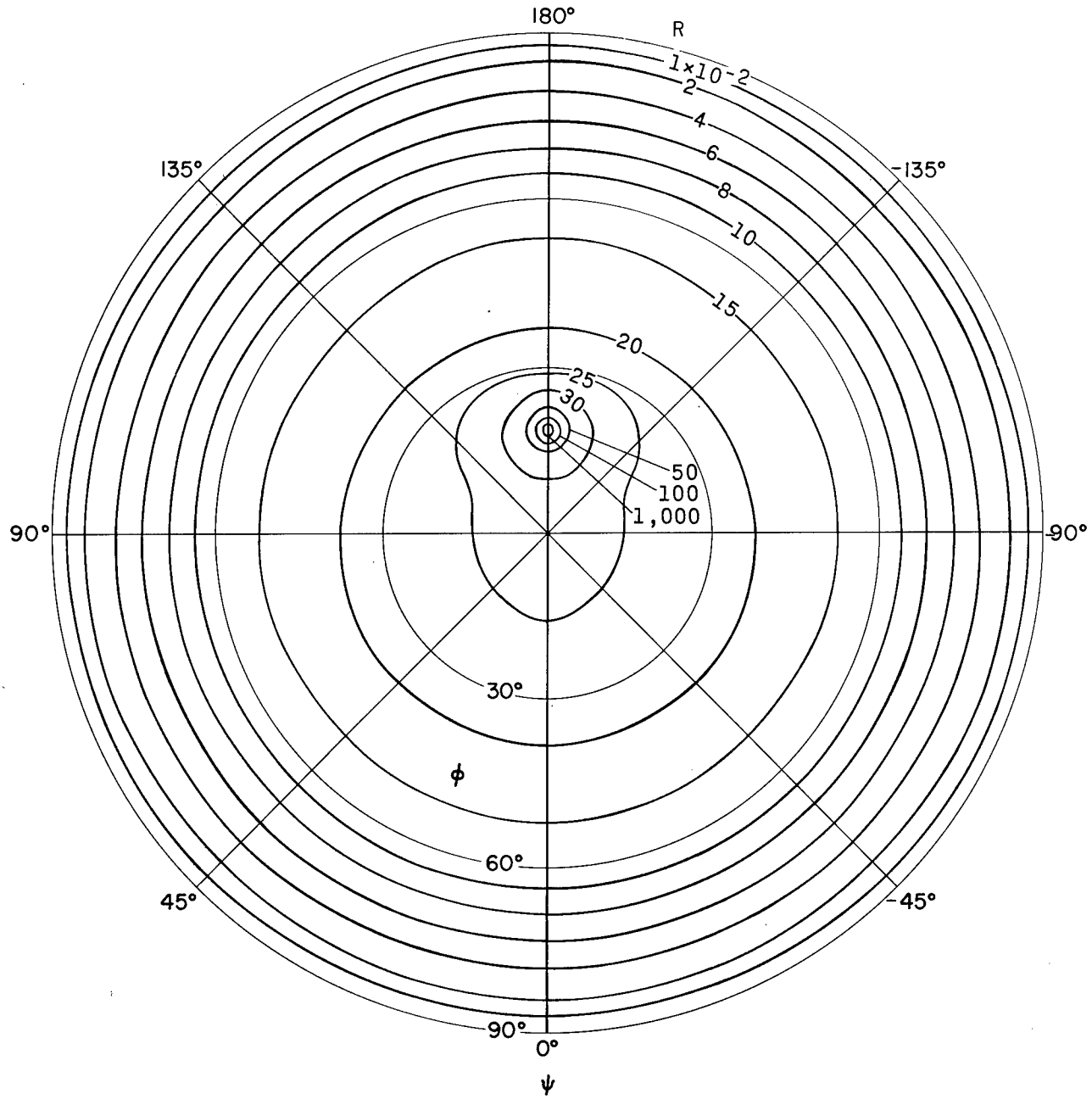

Figure 8.- Contour plot of reflectance of white paint for $i = 18.4^{\circ}$.

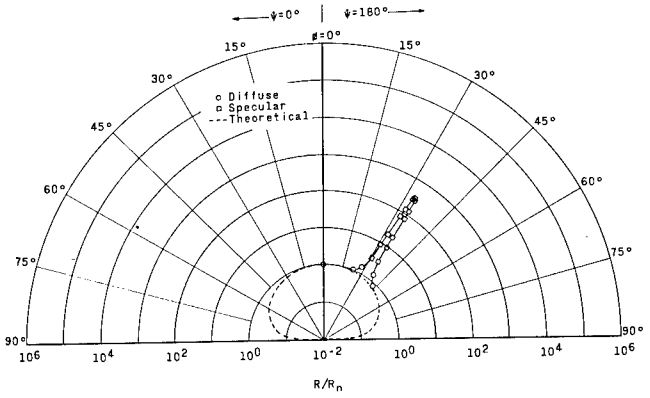

(a) Reflectance in plane of incidence.

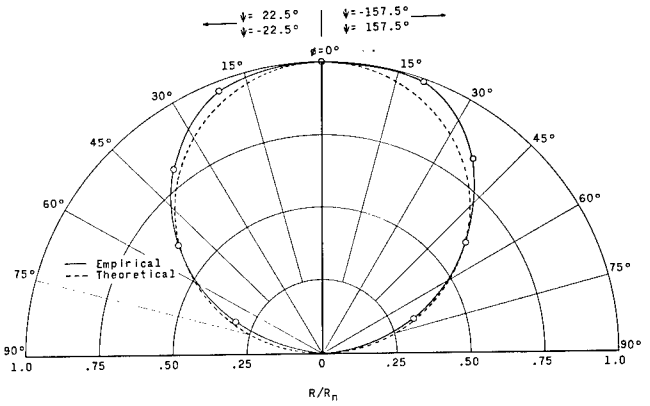

(b) Reflectance in plane displaced 22.5° from plane of incidence.

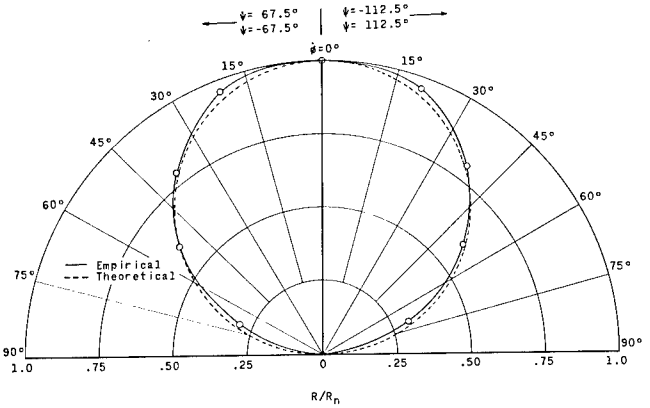

(c) Reflectance in plane displaced 67.5° from plane of incidence.

Figure 9.- Planar reflectance of white paint as a function of ϕ for $i = 33.2^{\circ}$.

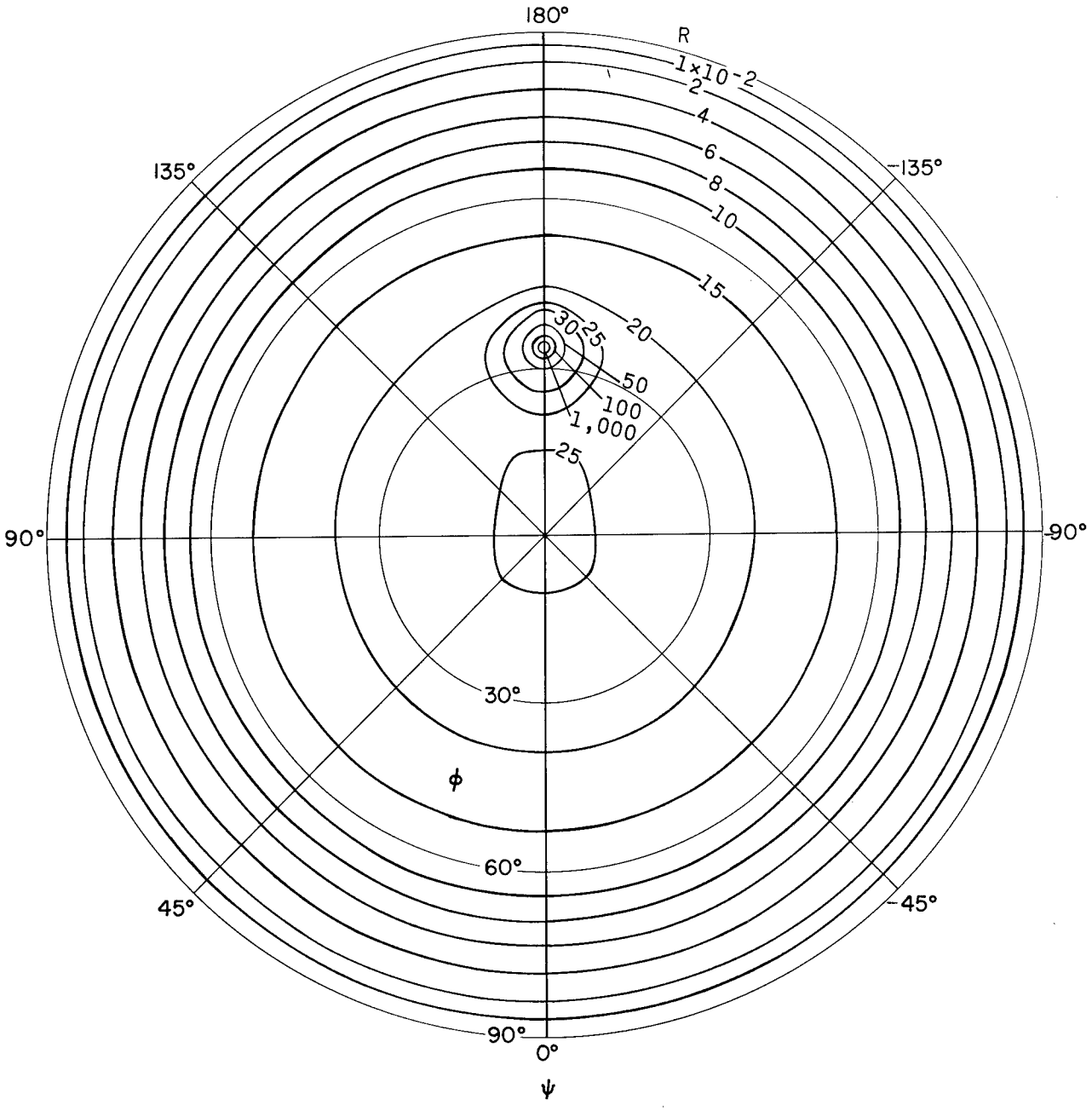

Figure 10.- Contour plot of reflectance of white paint for $i = 33.2^{\circ}$.

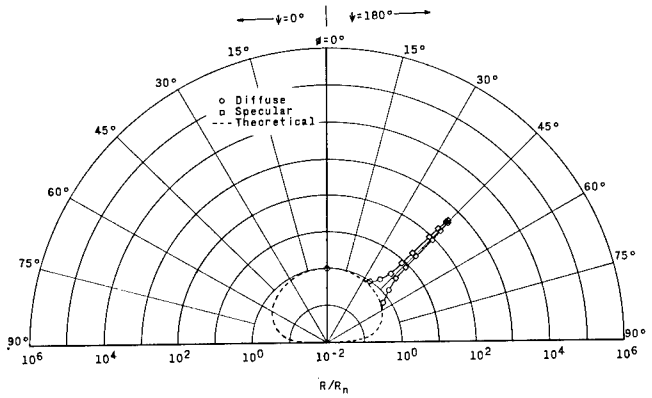

(a) Reflectance in plane of incidence.

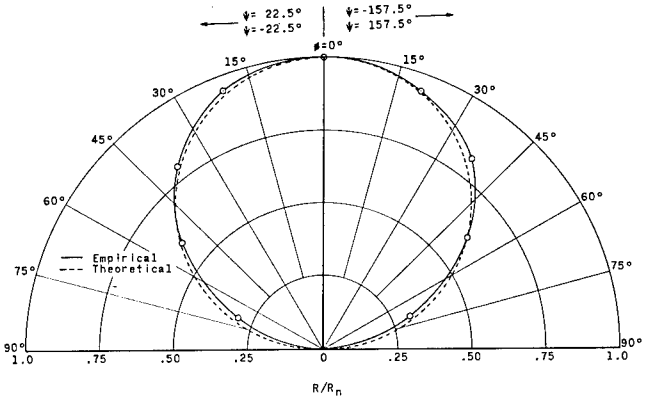

(b) Reflectance in plane displaced 22.5° from plane of incidence.

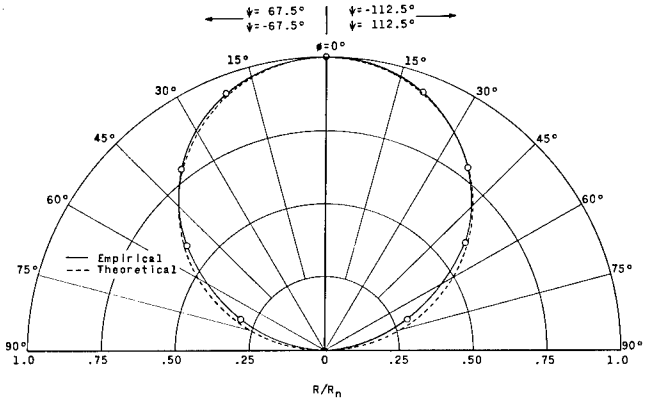

(c) Reflectance in plane displaced 67.5° from plane of incidence.

Figure 11.- Planar reflectance of white paint as a function of ϕ for $i = 45.0°$.

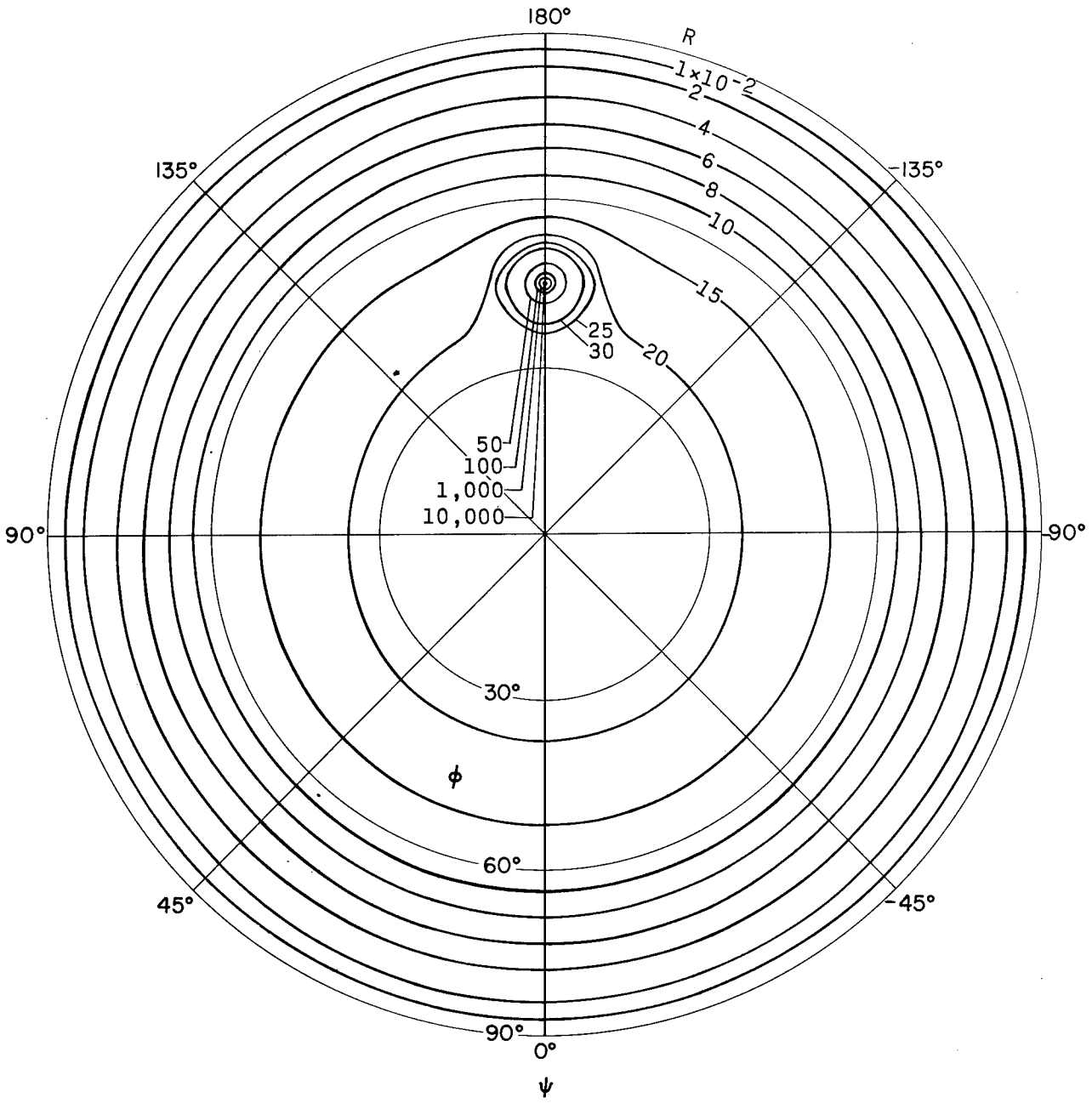

Figure 12.- Contour plot of reflectance of white paint for $i = 45.0^{\circ}$.

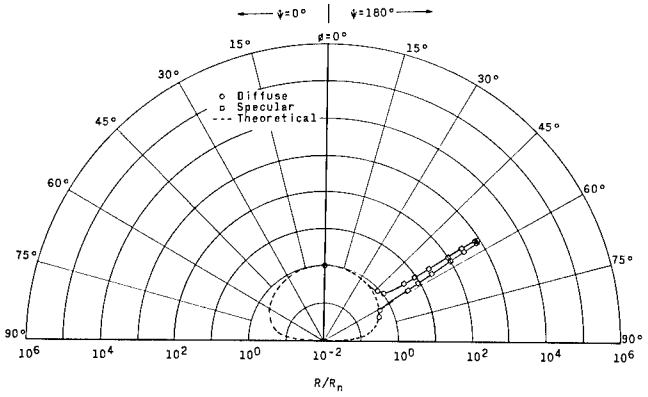

(a) Reflectance in plane of incidence.

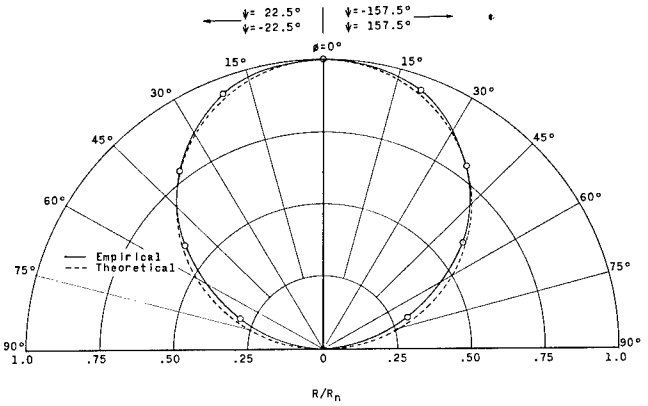

(b) Reflectance in plane displaced 22.5° from plane of incidence.

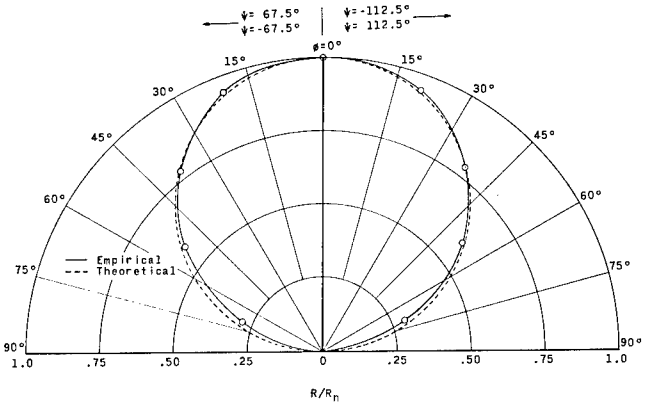

(c) Reflectance in plane displaced 67.5° from plane of incidence.

Figure 13.- Planar reflectance of white paint as a function of ϕ for $i = 56.8^{\circ}$.

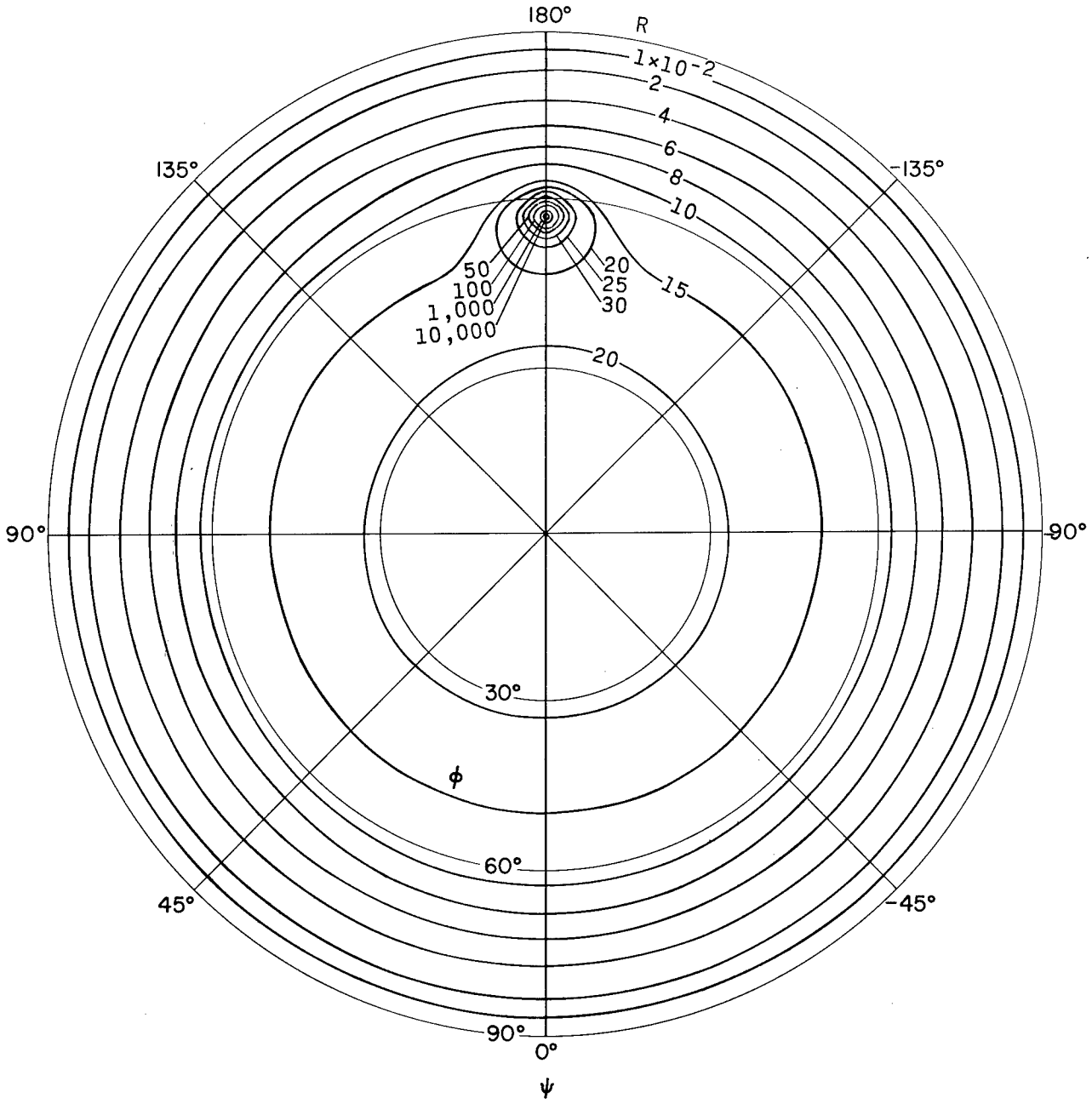

Figure 14.- Contour plot of reflectance of white paint for $i = 56.8^{\circ}$.

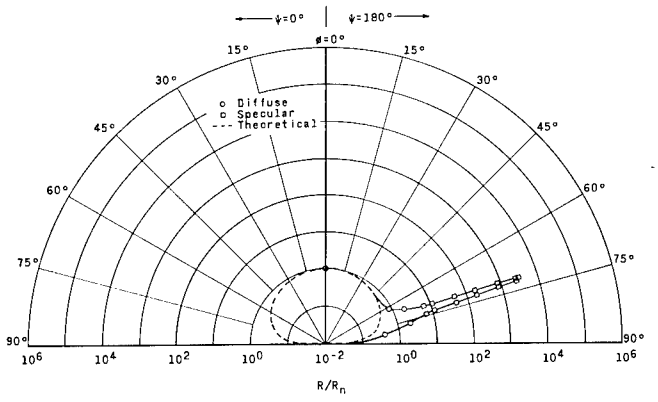

(a) Reflectance in plane of incidence.

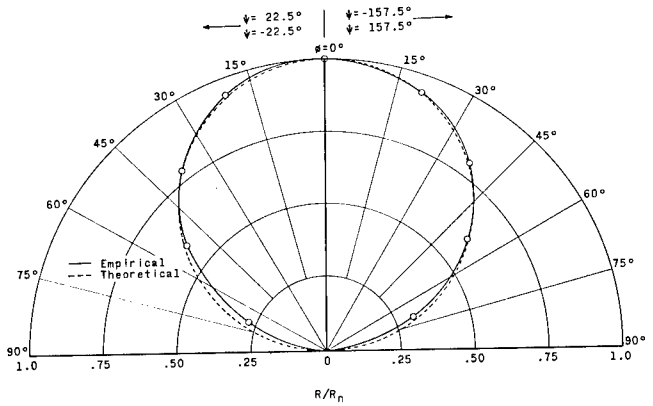

(b) Reflectance in plane displaced 22.5° from plane of incidence.

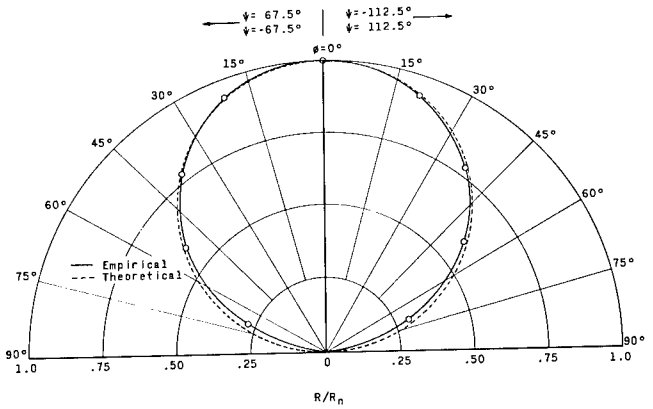

(c) Reflectance in plane displaced 67.5° from plane of incidence.

Figure 15.- Planar reflectance of white paint as a function of ϕ for $i = 71.6^{\circ}$.

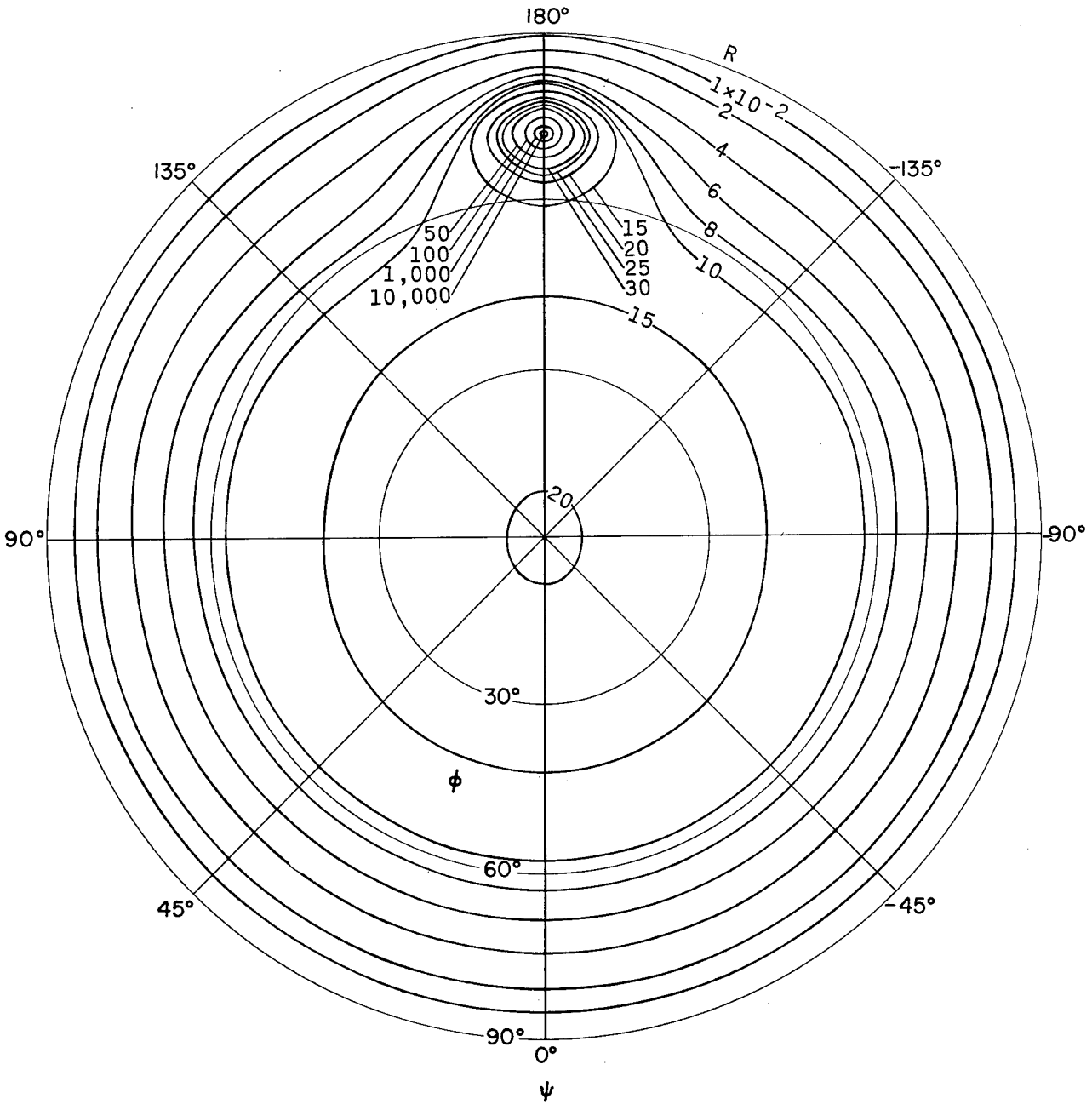

Figure 16.- Contour plot of reflectance of white paint for i = 71.6°.

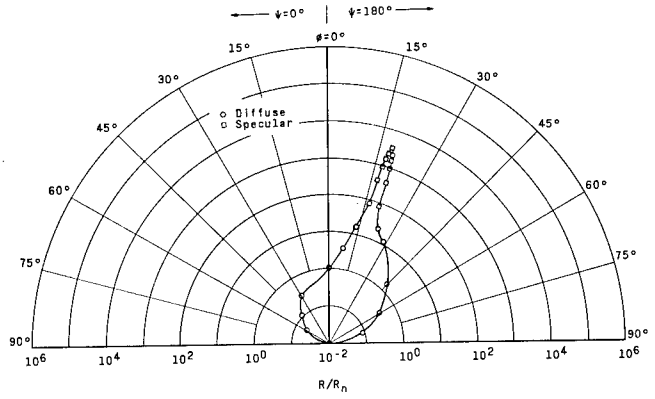

(a) Reflectance in plane of incidence.

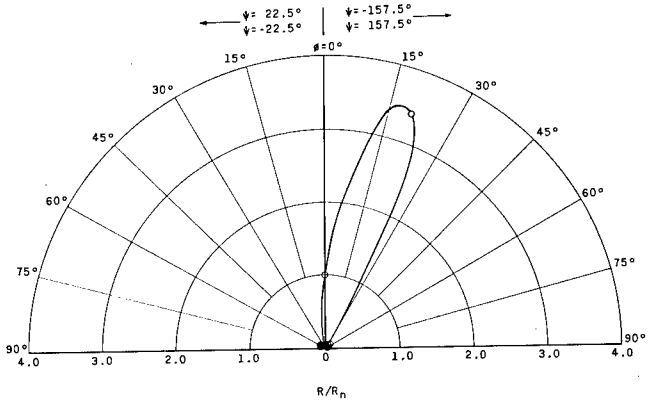

(b) Reflectance in plane displaced 22.5° from plane of incidence.

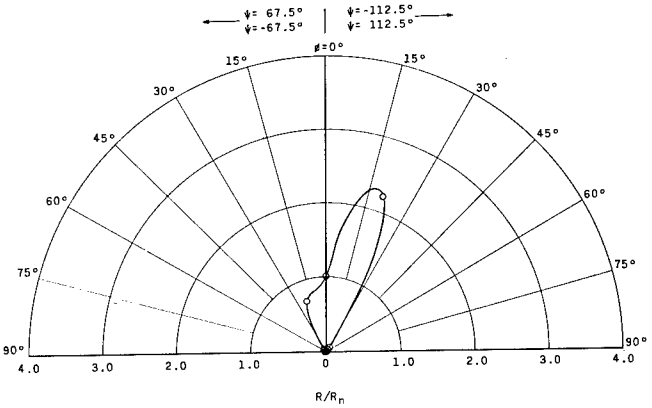

(c) Reflectance in plane displaced 67.5° from plane of incidence.

Figure 17.- Planar reflectance of aluminum as a function of ϕ for i = 18.4°.

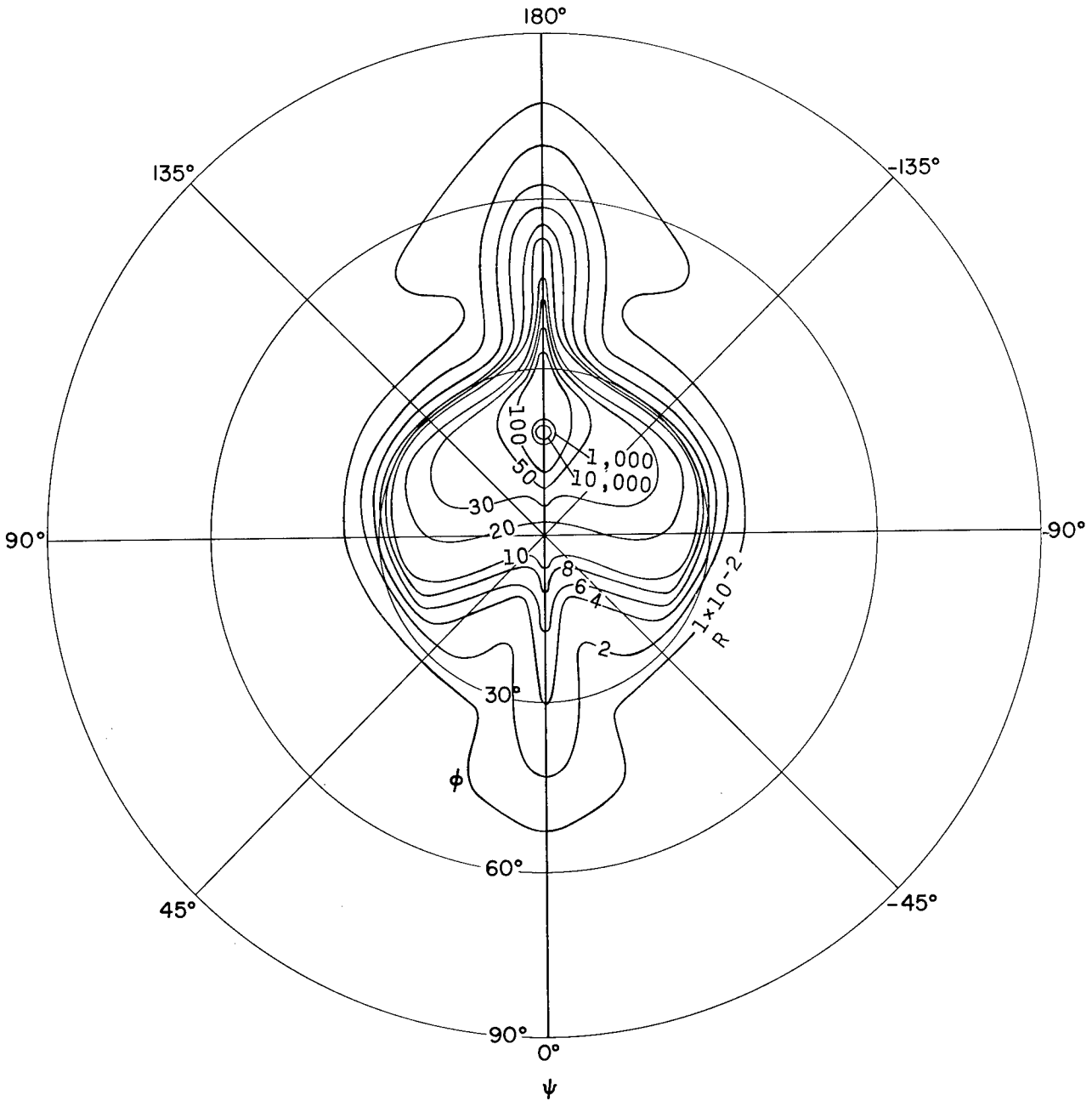

Figure 18.- Contour plot of reflectance of aluminum for $i = 18.4^{\circ}$.

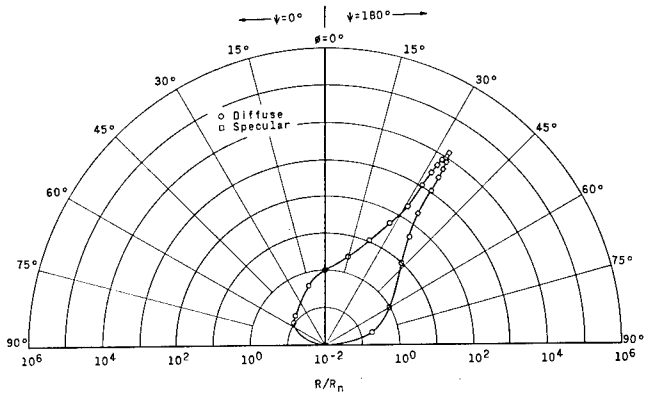

(a) Reflectance in plane of incidence.

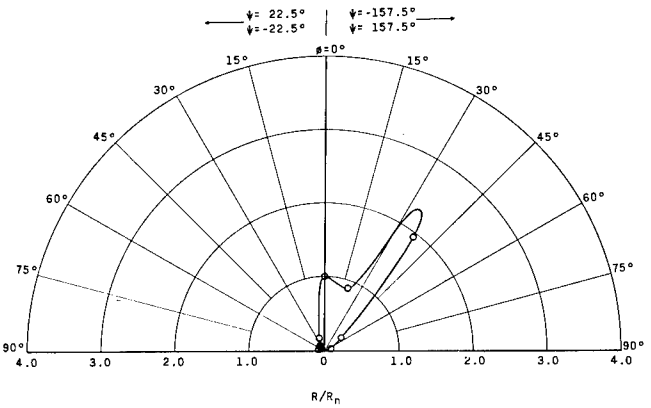

(b) Reflectance in plane displaced 22.5° from plane of incidence.

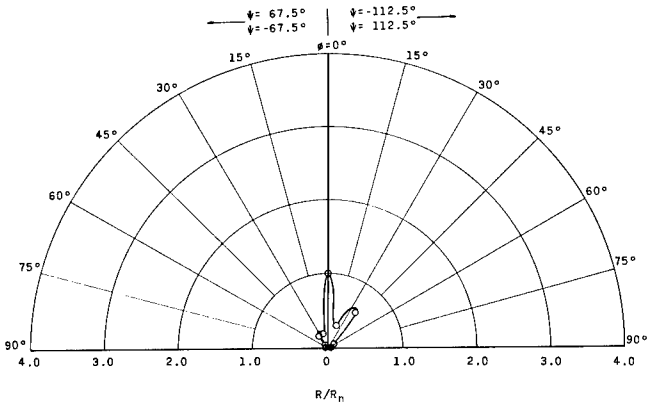

(c) Reflectance in plane displaced 67.5° from plane of incidence.

Figure 19.- Planar reflectance of aluminum as a function of ϕ for $i = 33.2^{\circ}$.

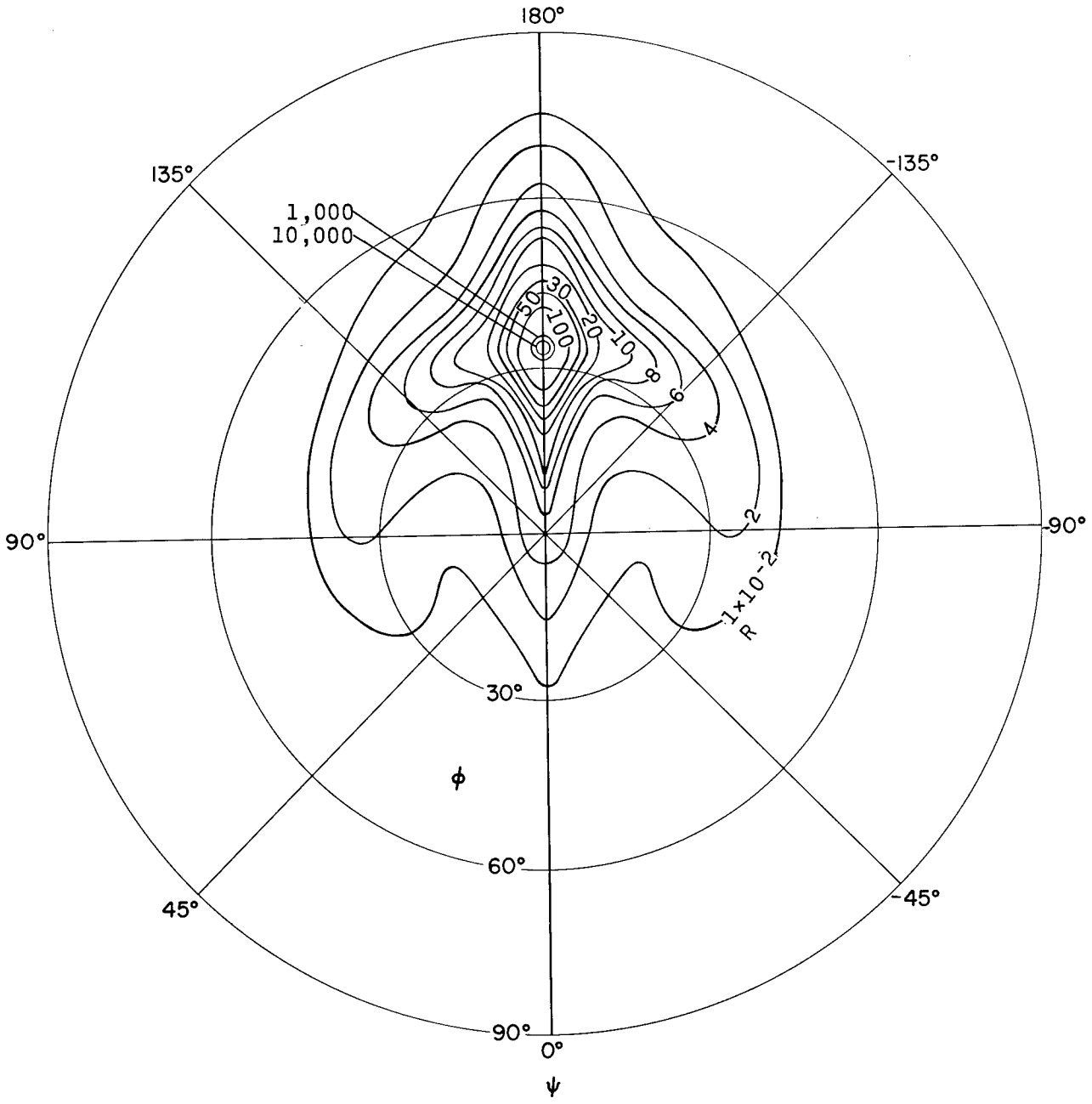

Figure 20.- Contour plot of reflectance of aluminum for $i = 33.2^{\circ}$.

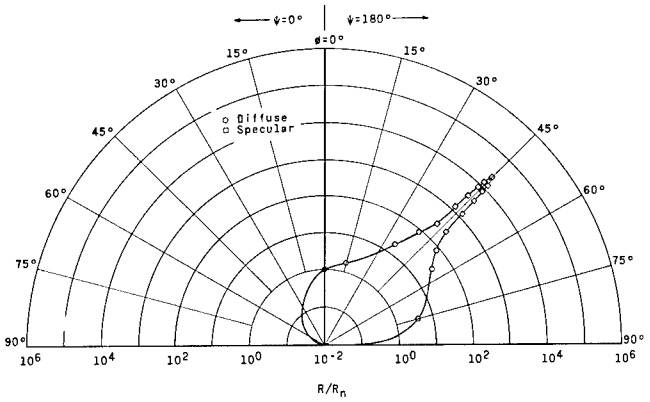

(a) Reflectance in plane of incidence.

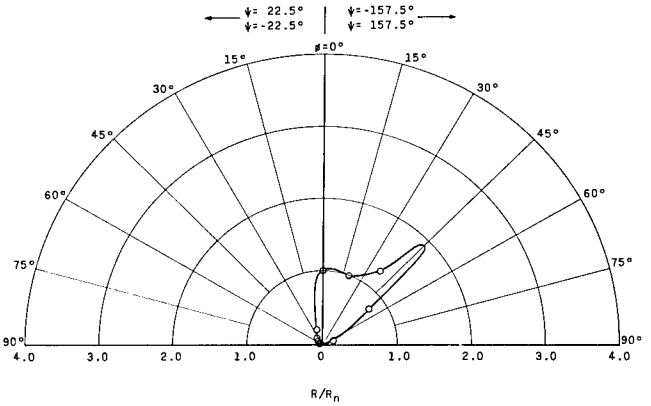

(b) Reflectance in plane displaced 22.5° from plane of incidence.

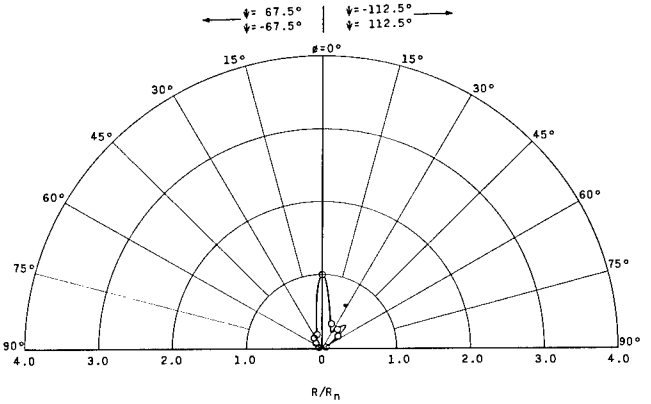

(c) Reflectance in plane displaced 67.5° from plane of incidence.

Figure 21.- Planar reflectance of aluminum as a function of ϕ for $i = 45.0°$.

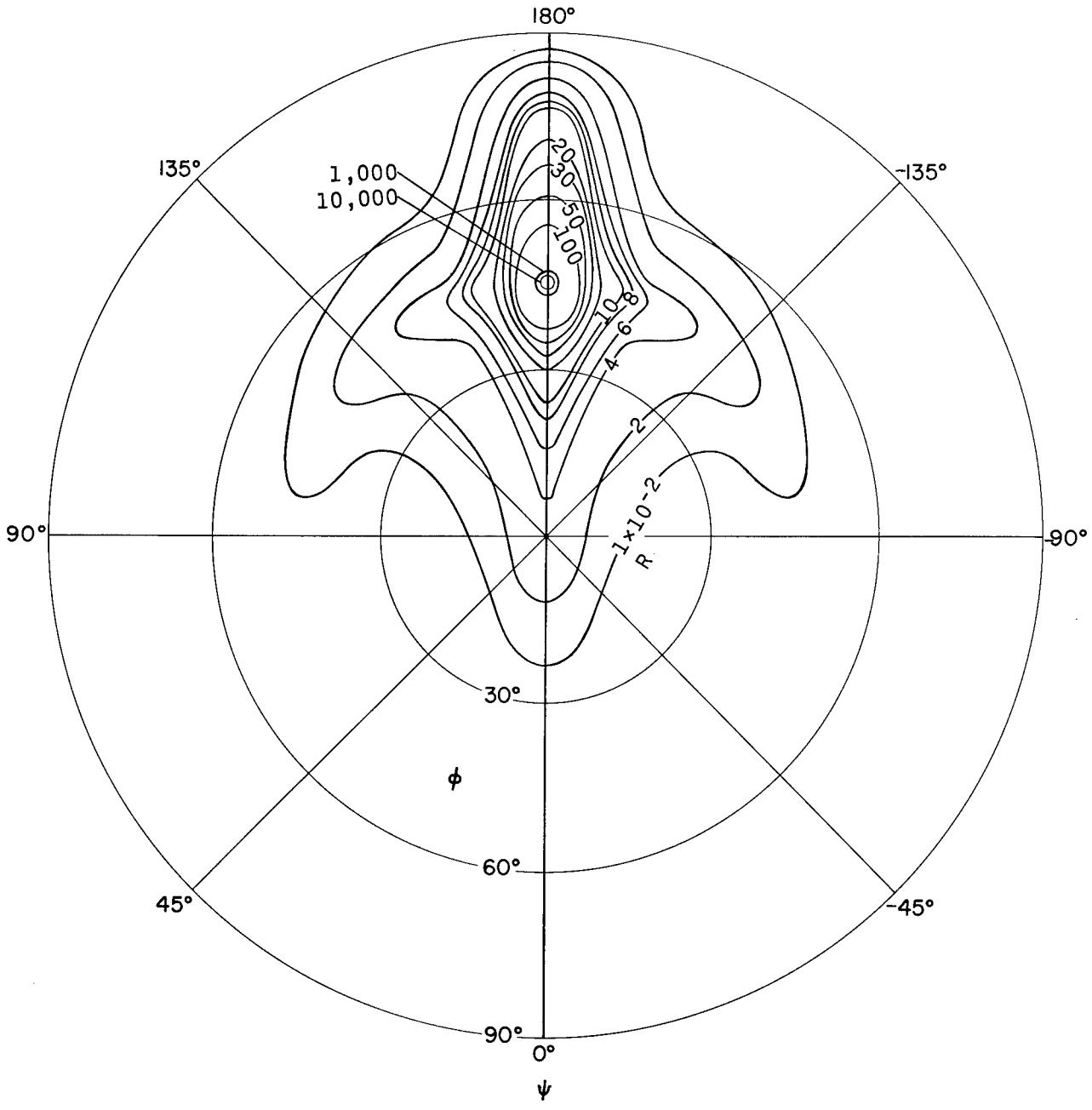

Figure 22.- Contour plot of reflectance of aluminum for i = 45.0°.

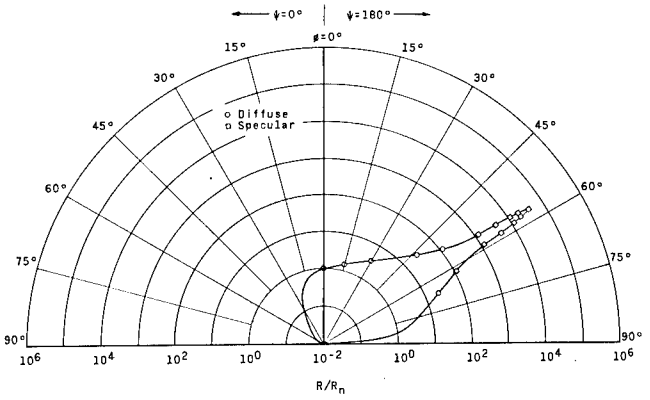

(a) Reflectance in plane of incidence.

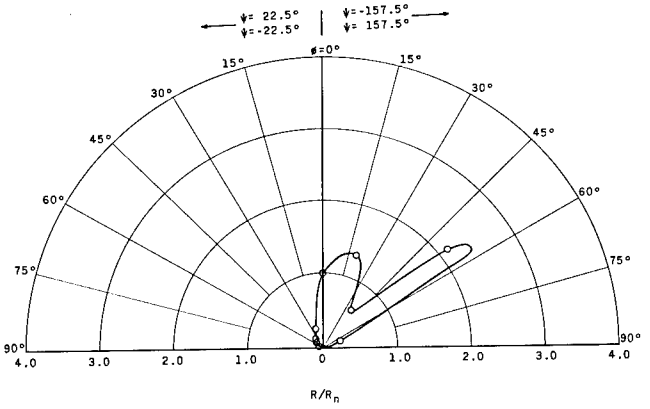

(b) Reflectance in plane displaced 22.5° from plane of incidence.

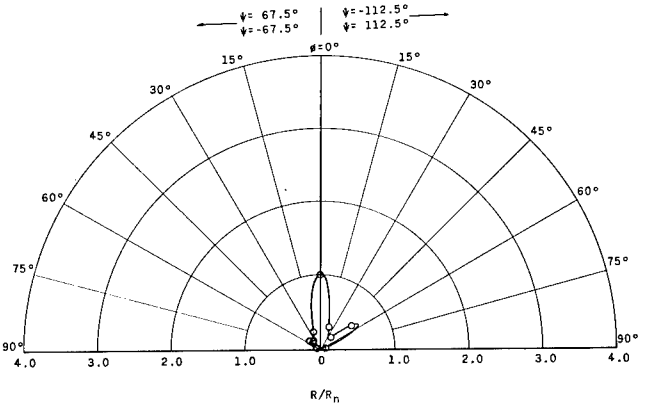

(c) Reflectance in plane displaced 67.5° from plane of incidence.

Figure 23.- Planar reflectance of aluminum as a function of ϕ for $i = 56.8^{\circ}$.

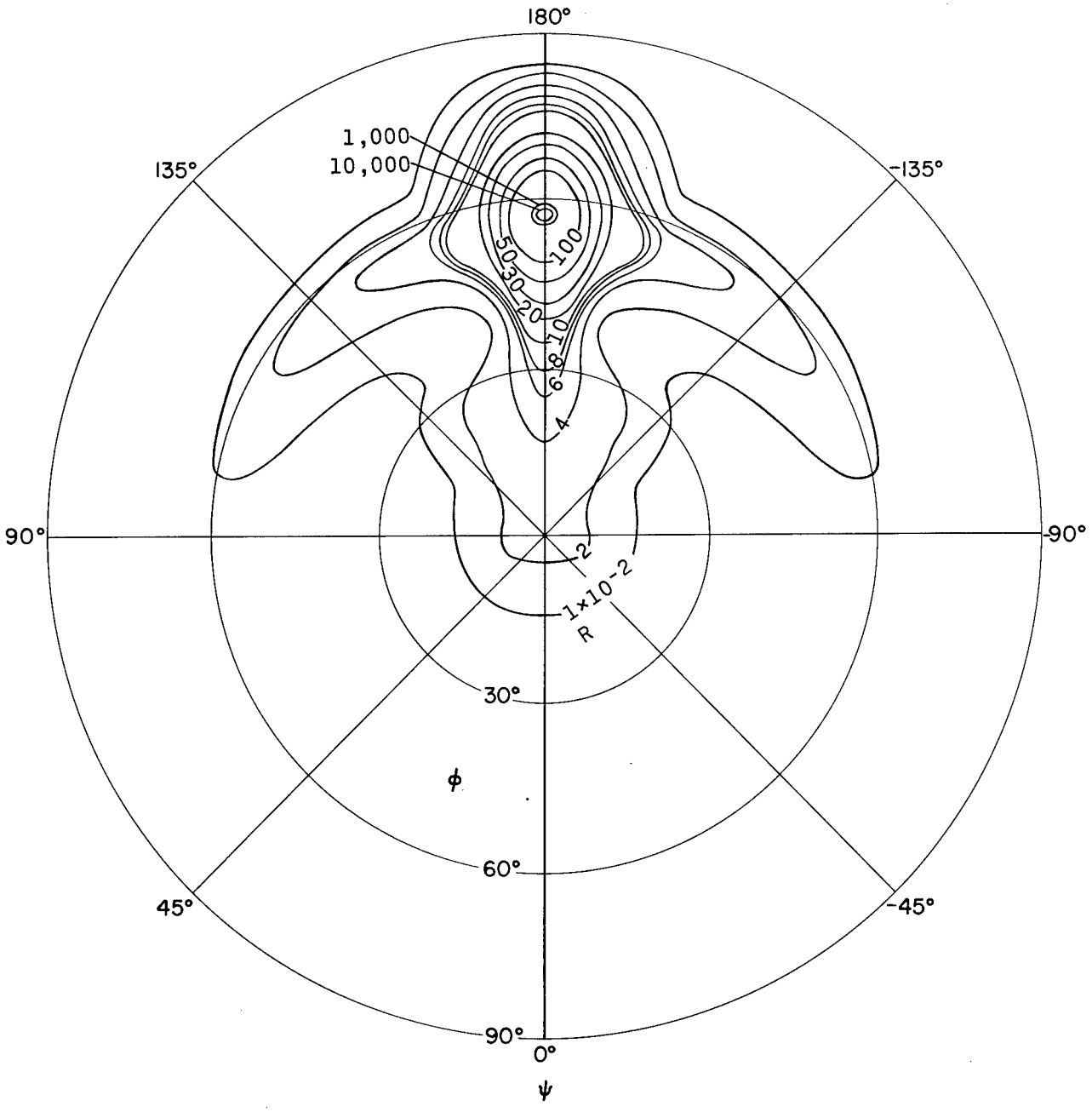

Figure 24.- Contour plot of reflectance of aluminum for $i = 56.8^{\circ}$.

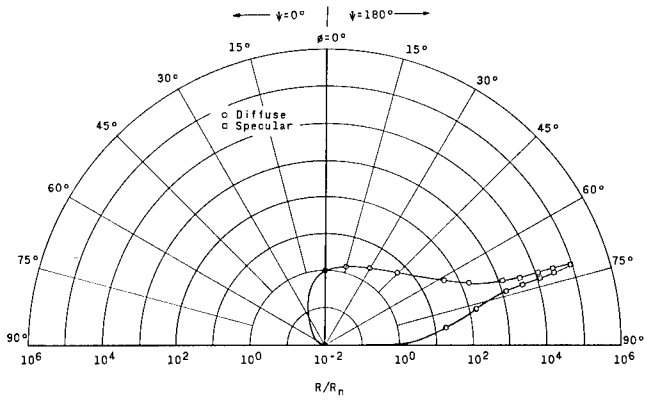

(a) Reflectance in plane of incidence.

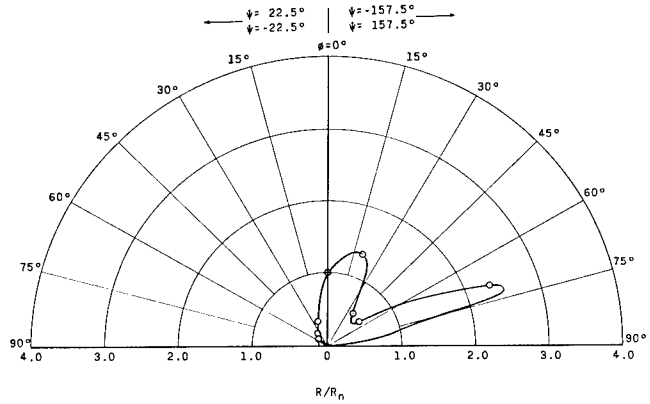

(b) Reflectance in plane displaced 22.5° from plane of incidence.

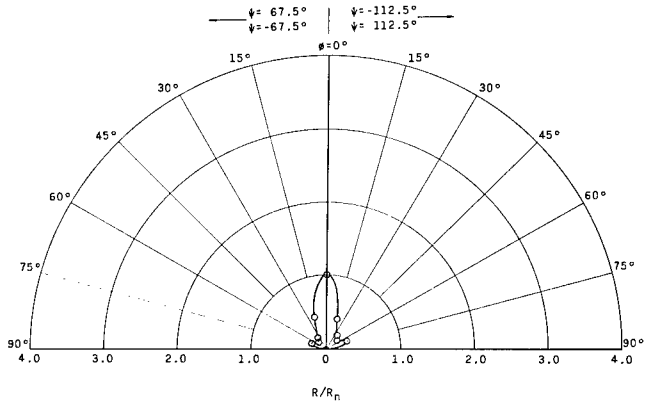

(c) Reflectance in plane displaced 67.5° from plane of incidence.

Figure 25.- Planar reflectance of aluminum as a function of ϕ for $i = 71.6^{\circ}$.

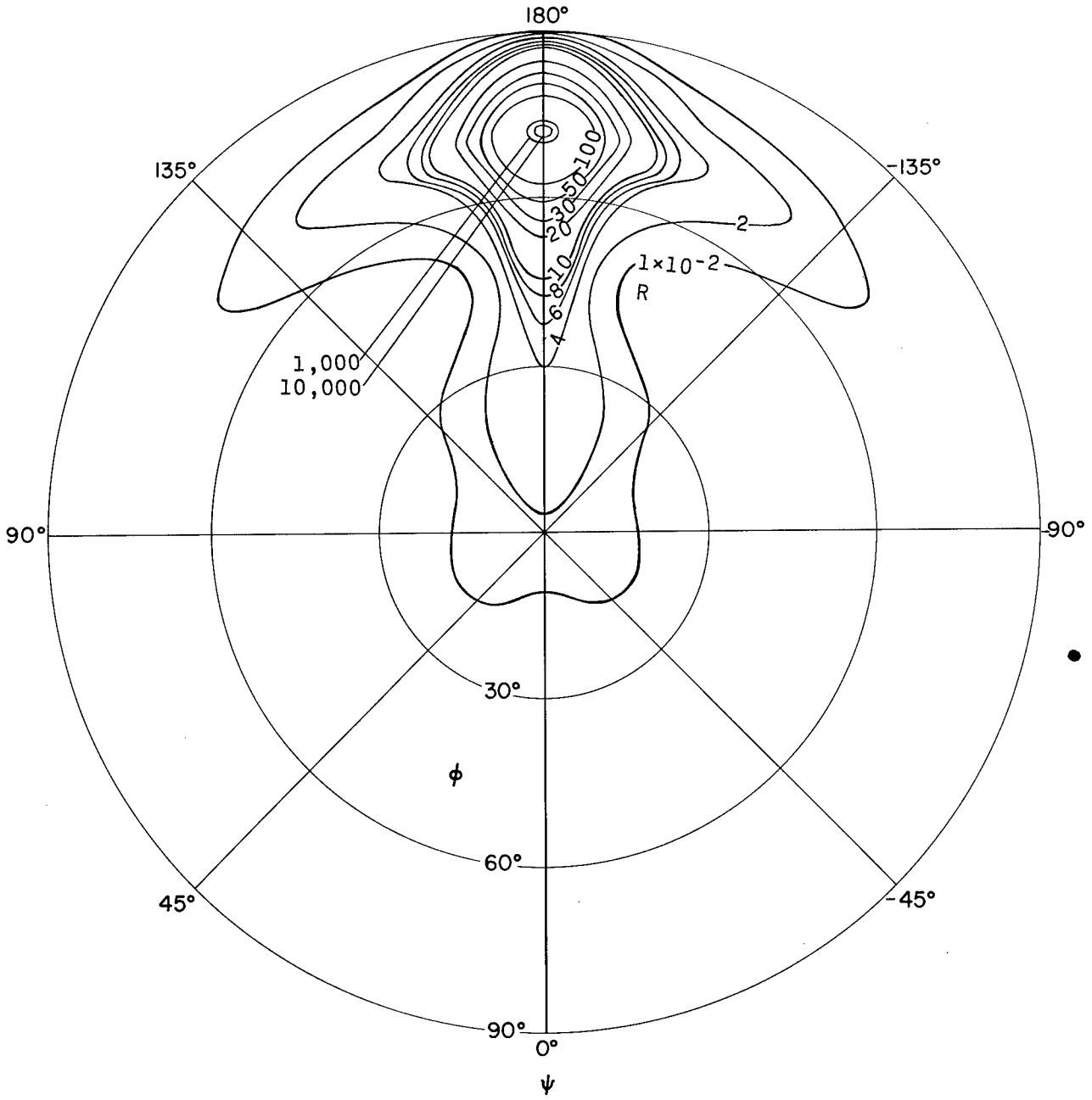

Figure 26.- Contour plot of reflectance of aluminum for i = 71.6°.

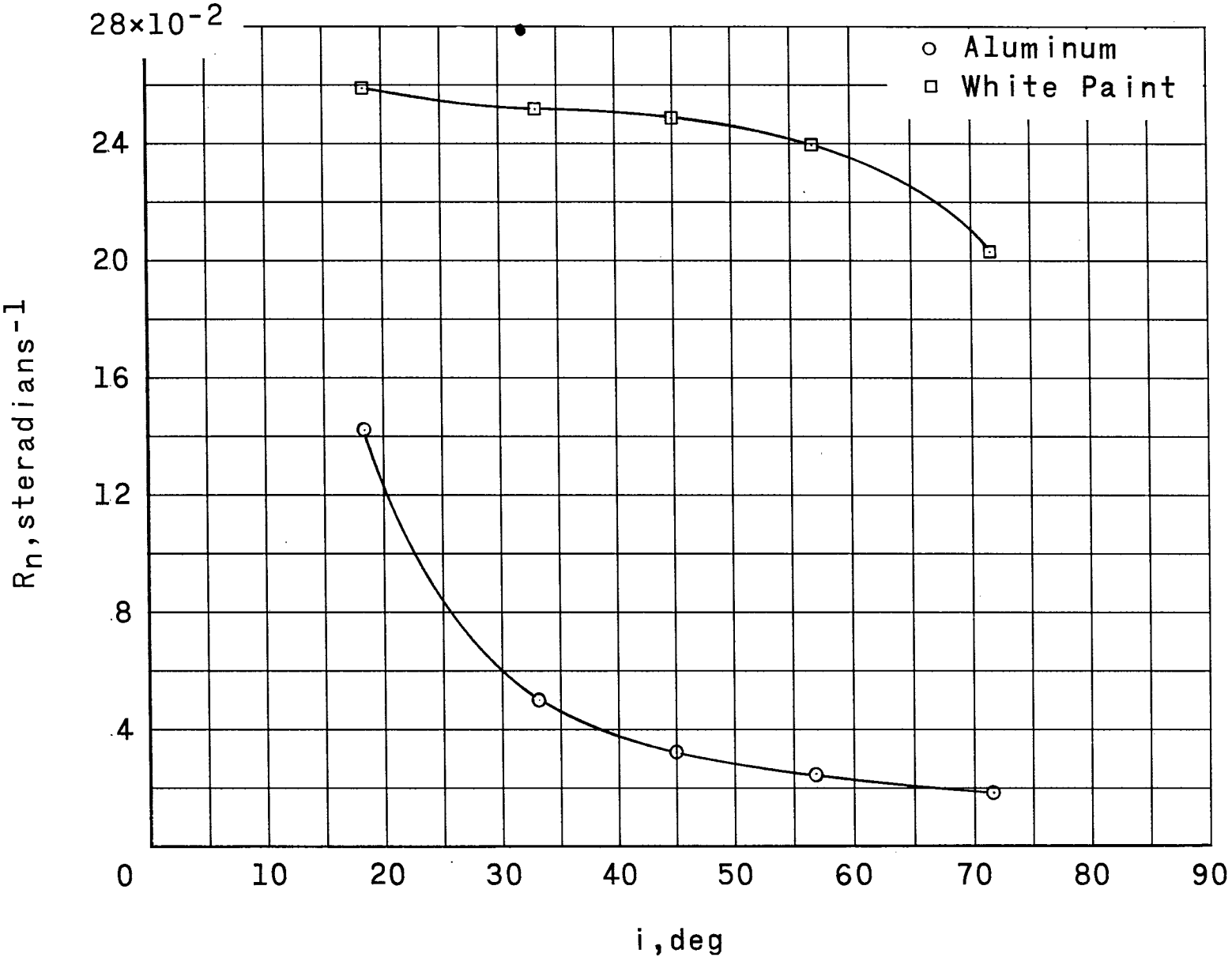

Figure 27.- Normal reflectance of white paint and aluminum as a function of angle of incidence.

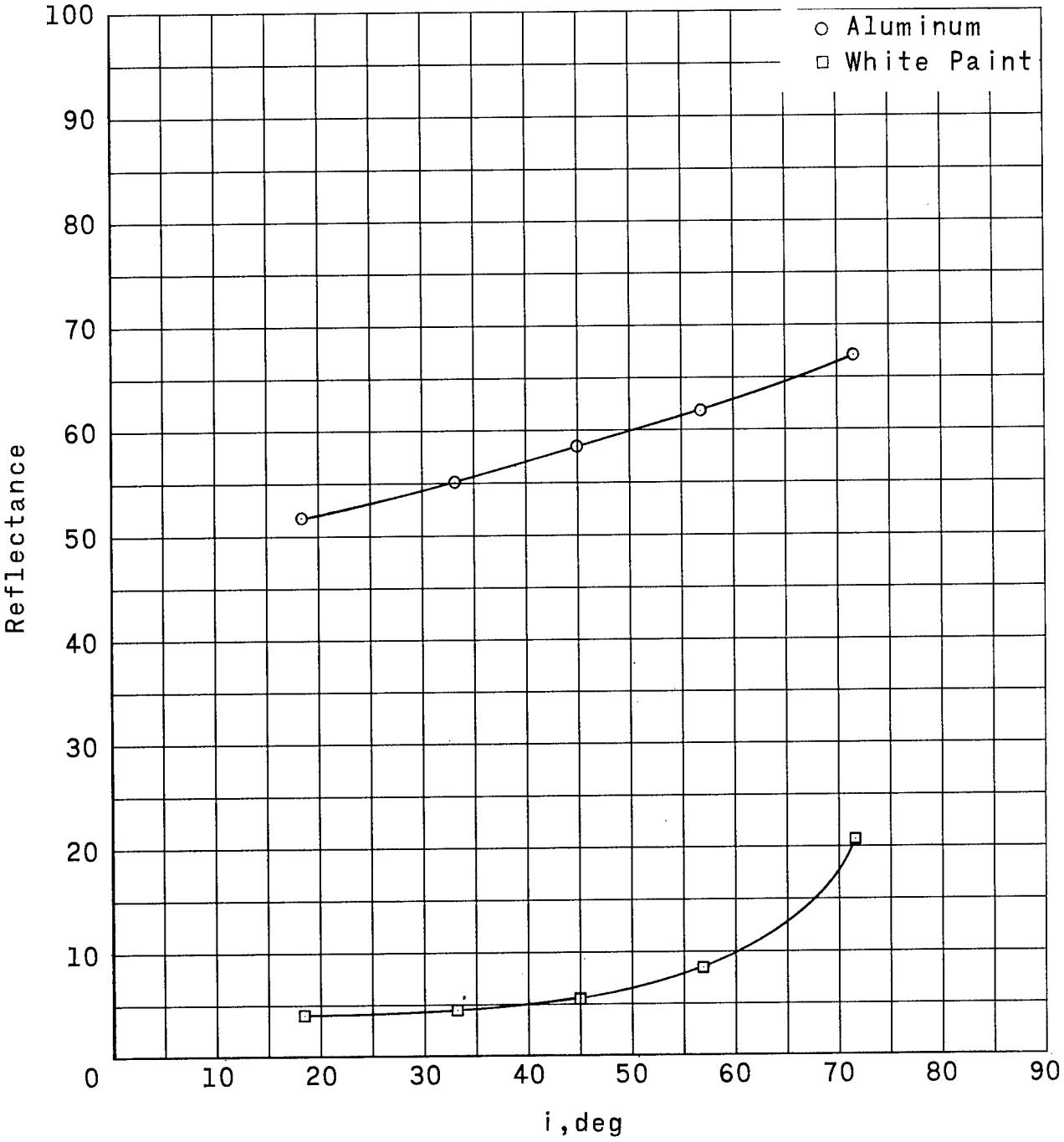

Figure 28.- Total reflectance within 2.5° of angle of specular reflection as a function of angle of incidence.

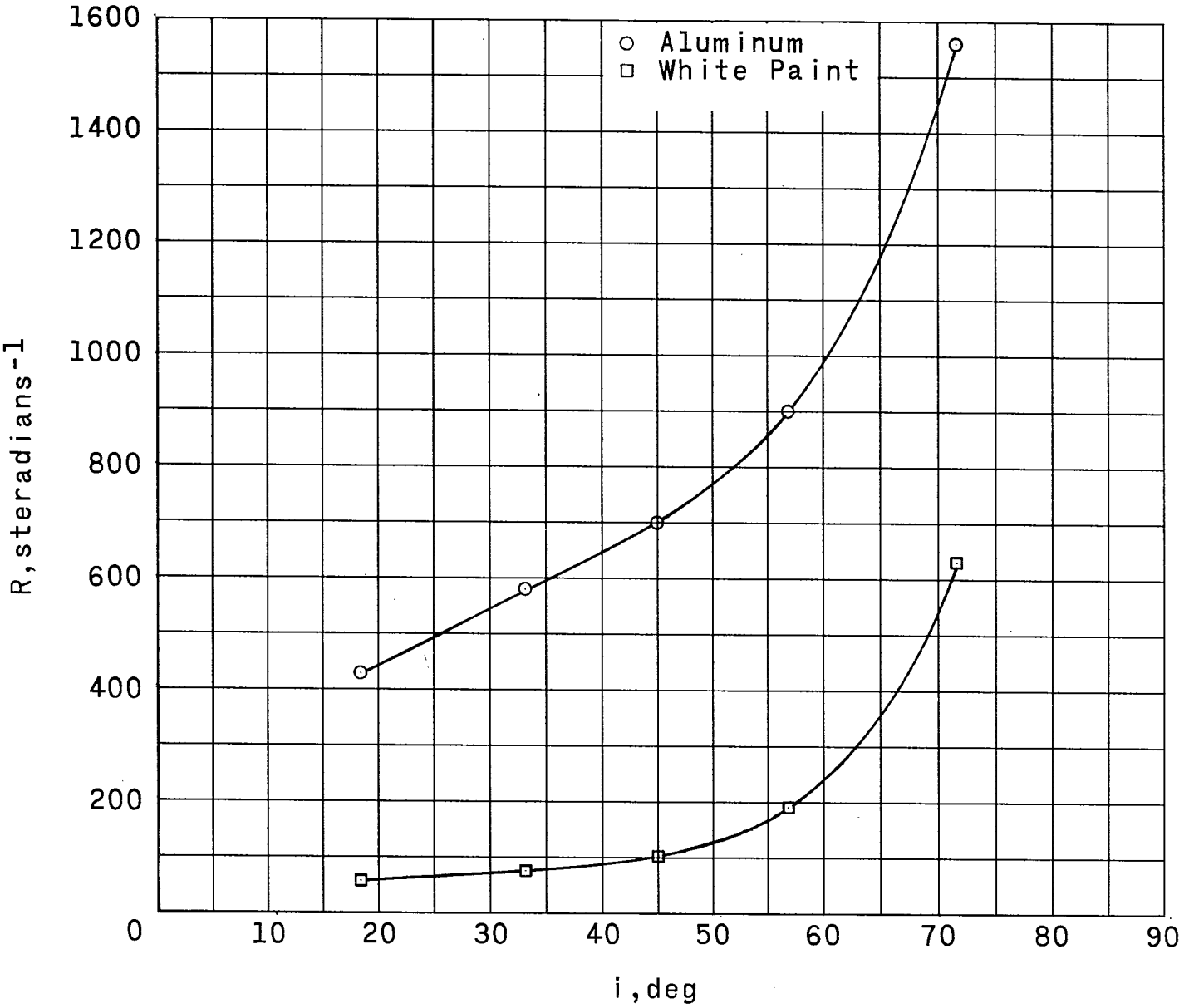

Figure 29.- Reflectance per unit solid angle at angle of specular reflection as a function of angle of incidence.

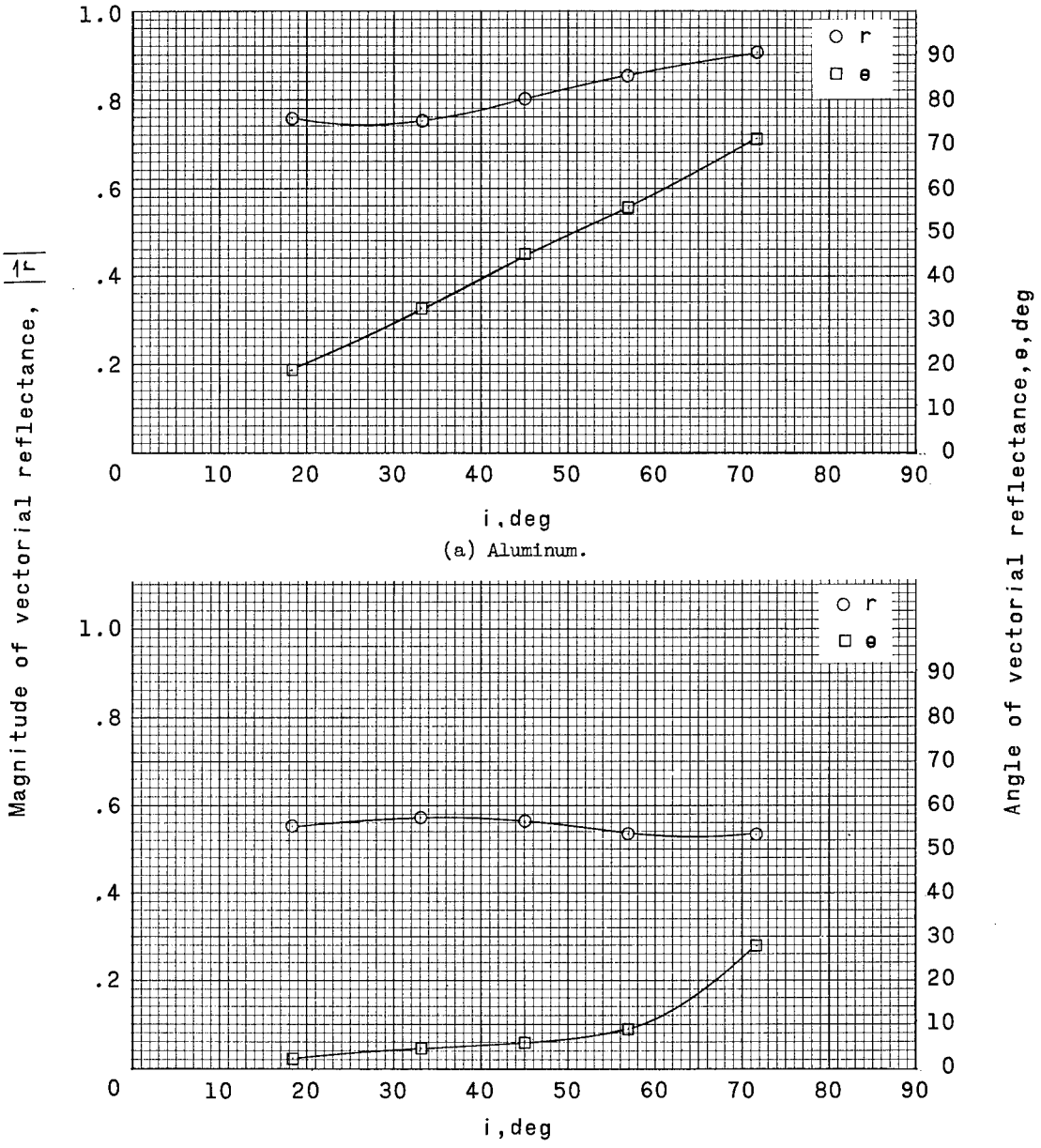

(a) Aluminum.

(b) White epoxy paint.

Figure 30.- Vectorial reflectance of aluminum and white epoxy paint samples as a function of angle of incidence.

NASA TN D-2388
National Aeronautics and Space Administration.
VECTORIAL REFLECTANCE OF THE EXPLORER IX SATELLITE MATERIAL. Gerald M. Keating and James A. Mullins. August 1964. 45p. OTS price, $1.25. (NASA TECHNICAL NOTE D-2388)

Reflectance measurements were made at different azimuth and colatitude angles relative to flat samples of the aluminum and white epoxy paint surfaces used on the Explorer IX satellite. These measurements were made by an adapted monoplanar goniophotometer. The total vectorial reflectance of the samples for different angles of incidence was obtained by vectorial summation of the reflected light flux.

I. Keating, Gerald M.
II. Mullins, James A.
III. NASA TN D-2388

NASA

NASA TN D-2388
National Aeronautics and Space Administration.
VECTORIAL REFLECTANCE OF THE EXPLORER IX SATELLITE MATERIAL. Gerald M. Keating and James A. Mullins. August 1964. 45p. OTS price, $1.25. (NASA TECHNICAL NOTE D-2388)

Reflectance measurements were made at different azimuth and colatitude angles relative to flat samples of the aluminum and white epoxy paint surfaces used on the Explorer IX satellite. These measurements were made by an adapted monoplanar goniophotometer. The total vectorial reflectance of the samples for different angles of incidence was obtained by vectorial summation of the reflected light flux.

I. Keating, Gerald M.
II. Mullins, James A.
III. NASA TN D-2388

NASA

NASA TN D-2388
National Aeronautics and Space Administration.
VECTORIAL REFLECTANCE OF THE EXPLORER IX SATELLITE MATERIAL. Gerald M. Keating and James A. Mullins. August 1964. 45p. OTS price, $1.25. (NASA TECHNICAL NOTE D-2388)

Reflectance measurements were made at different azimuth and colatitude angles relative to flat samples of the aluminum and white epoxy paint surfaces used on the Explorer IX satellite. These measurements were made by an adapted monoplanar goniophotometer. The total vectorial reflectance of the samples for different angles of incidence was obtained by vectorial summation of the reflected light flux.

I. Keating, Gerald M.
II. Mullins, James A.
III. NASA TN D-2388

NASA

NASA TN D-2388
National Aeronautics and Space Administration.
VECTORIAL REFLECTANCE OF THE EXPLORER IX SATELLITE MATERIAL. Gerald M. Keating and James A. Mullins. August 1964. 45p. OTS price, $1.25. (NASA TECHNICAL NOTE D-2388)

Reflectance measurements were made at different azimuth and colatitude angles relative to flat samples of the aluminum and white epoxy paint surfaces used on the Explorer IX satellite. These measurements were made by an adapted monoplanar goniophotometer. The total vectorial reflectance of the samples for different angles of incidence was obtained by vectorial summation of the reflected light flux.

I. Keating, Gerald M.
II. Mullins, James A.
III. NASA TN D-2388

NASA

"The aeronautical and space activities of the United States shall be conducted so as to contribute . . . to the expansion of human knowledge of phenomena in the atmosphere and space. The Administration shall provide for the widest practicable and appropriate dissemination of information concerning its activities and the results thereof."

—NATIONAL AERONAUTICS AND SPACE ACT OF 1958

NASA SCIENTIFIC AND TECHNICAL PUBLICATIONS

TECHNICAL REPORTS: Scientific and technical information considered important, complete, and a lasting contribution to existing knowledge.

TECHNICAL NOTES: Information less broad in scope but nevertheless of importance as a contribution to existing knowledge.

TECHNICAL MEMORANDUMS: Information receiving limited distribution because of preliminary data, security classification, or other reasons.

CONTRACTOR REPORTS: Technical information generated in connection with a NASA contract or grant and released under NASA auspices.

TECHNICAL TRANSLATIONS: Information published in a foreign language considered to merit NASA distribution in English.

TECHNICAL REPRINTS: Information derived from NASA activities and initially published in the form of journal articles.

SPECIAL PUBLICATIONS: Information derived from or of value to NASA activities but not necessarily reporting the results of individual NASA-programmed scientific efforts. Publications include conference proceedings, monographs, data compilations, handbooks, sourcebooks, and special bibliographies.

Details on the availability of these publications may be obtained from:

SCIENTIFIC AND TECHNICAL INFORMATION DIVISION

NATIONAL AERONAUTICS AND SPACE ADMINISTRATION

Washington, D.C. 20546